

# Electron Transfer Mechanisms of DNA Repair by Photolyase

Dongping Zhong

Department of Physics, Department of Chemistry and Biochemistry, and Programs of Biophysics, Chemical Physics, and Biochemistry, The Ohio State University, Columbus, Ohio 43210; email: zhong.28@osu.edu

Annu. Rev. Phys. Chem. 2015. 66:691–715

The *Annual Review of Physical Chemistry* is online at [physchem.annualreviews.org](http://physchem.annualreviews.org)

This article's doi:  
10.1146/annurev-physchem-040513-103631

Copyright © 2015 by Annual Reviews.  
All rights reserved

## Keywords

nonequilibrium ultrafast dynamics, dimer sequential splitting, electron tunneling pathway, high repair efficiency, flavin functional state, proton-coupled electron transfer

## Abstract

Photolyase is a flavin photoenzyme that repairs two DNA base damage products induced by ultraviolet (UV) light: cyclobutane pyrimidine dimers and 6-4 photoproducts. With femtosecond spectroscopy and site-directed mutagenesis, investigators have recently made significant advances in our understanding of UV-damaged DNA repair, and the entire enzymatic dynamics can now be mapped out in real time. For dimer repair, six elementary steps have been characterized, including three electron transfer reactions and two bond-breaking processes, and their reaction times have been determined. A unique electron-tunneling pathway was identified, and the critical residues in modulating the repair function at the active site were determined. The dynamic synergy between the elementary reactions for maintaining high repair efficiency was elucidated, and the biological nature of the flavin active state was uncovered. For 6-4 photoproduct repair, a proton-coupled electron transfer repair mechanism has been revealed. The elucidation of electron transfer mechanisms and two repair photocycles is significant and provides a molecular basis for future practical applications, such as in rational drug design for curing skin cancer.

## 1. INTRODUCTION

The detrimental effect of ultraviolet (UV) radiation in sunlight is that it can cause DNA damage by inducing the formation of a cyclobutane pyrimidine dimer (CPD; ~80% of the total damage) or a pyrimidine-pyrimidone (6-4) photoproduct (6-4PP; ~20%) (**Figure 1a**) (1, 2). In a CPD, the two nearby thymine bases in the same DNA strand covalently connect to form a cyclobutane ring. Conversely, a 6-4PP has a complicated chemical structure in which the oxygen and hydrogen atoms in one base migrate to another base, and the two bases are covalently linked. Both UV photoproducts can lead to toxic mutagenesis, cell apoptosis, and even skin cancer (3, 4). Photolyases, a class of flavoproteins and photoenzymes in nature, repair those DNA lesions upon the absorption of blue light (**Figure 1b**) (5–7). Two types of photolyases with similar primary sequences and folding architectures (**Figure 1c,d**) specifically repair the two photoproducts, respectively. Both photolyases contain two noncovalently bound chromophores: One is a fully reduced flavin adenine

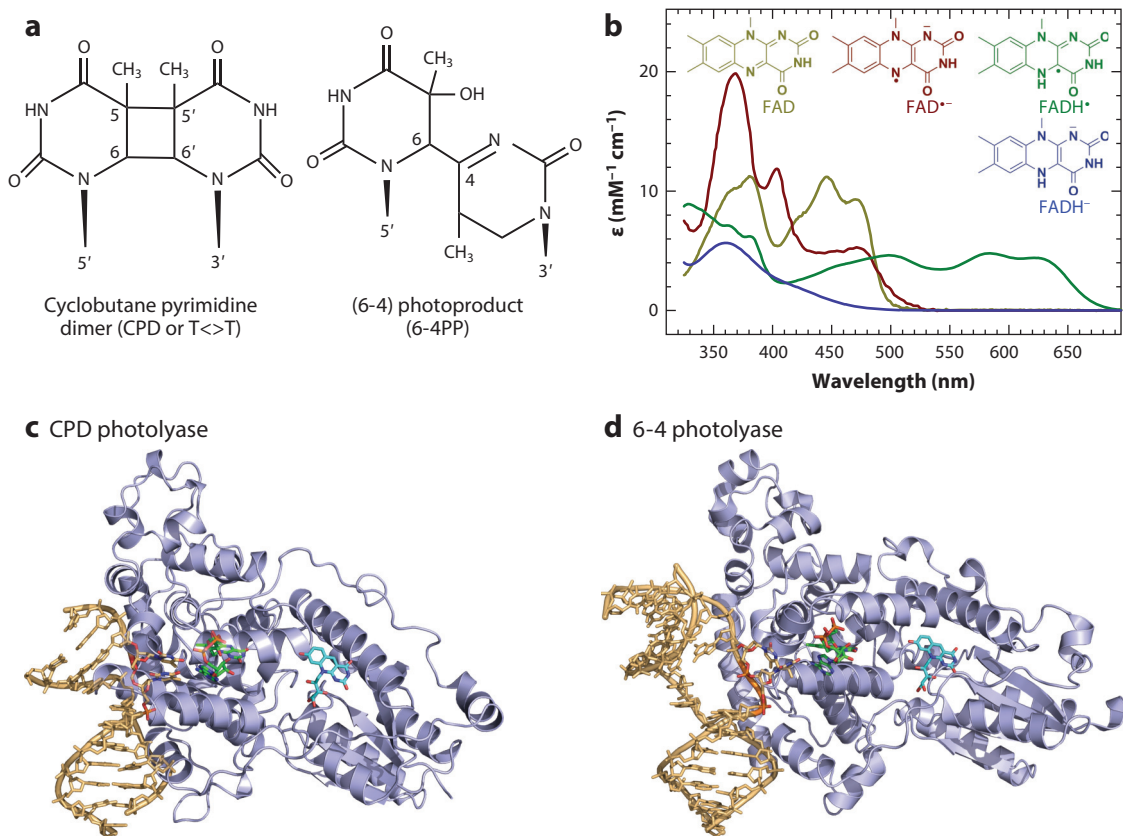


**Figure 1**

(a) Chemical structures of two UV-induced DNA photolesions. (b) Absorption spectra of four redox states of flavin adenine dinucleotide (FAD) and their corresponding structures. (c) Complex X-ray structure of *Anacystis nidulans* photolyase and DNA with an antenna molecule [8-hydroxy-7,8-didemethyl-5-deazariboflavin (8-HDF) or methenyltetrahydrofolate (MTHF) in *Escherichia coli* cyclobutane pyrimidine dimer (CPD) photolyase; cyan), a catalytic cofactor ( $\text{FADH}^{\cdot-}$ ; green), and a repaired photoproduct of the thymine dimer (yellow). (d) Complex X-ray structure of *Drosophila melanogaster* (6-4) photolyase and DNA with a light-harvesting antenna chromophore (8-HDF; cyan), a catalytic cofactor ( $\text{FADH}^{\cdot-}$ ; green), and a (6-4) photoproduct (6-4PP; yellow). Both the thymine dimer and 6-4PP are flipped out of the DNA and inserted into the active site.

dinucleotide (FADH<sup>-</sup>) molecule as the active cofactor (**Figure 1b**) (8, 9), and the other is either folate or 5-deazariboflavin as an antenna pigment (10, 11).

Photolyases have been extensively characterized both biochemically and structurally (7, 12, 13). Various biochemical studies were well reviewed by Sancar (7) in 2003, and recent structural characterizations have been summarized by Essen (12). Significant advances in the past decade have been made by solving the complex structures of photolyases with substrates (14–19). The earlier structure had an unusual U-shape folded configuration of the FADH<sup>-</sup> cofactor at the bottom of the active sites (20), and recent complex structures demonstrated that the adenine moiety lies between the isoalloxazine ring and the substrates at van der Waals distances and that the photolesions flip out of the double-stranded DNA and intrude into the active sites of photolyases with bent DNA structures (14, 19) (**Figure 1b**). Stuchebrukhov and colleagues (21) predicted such a complex configuration early on by using computational simulations before determining the X-ray structures. The repair mechanism of CPD lesions had been proposed and examined in the past few decades (7, 22, 23), but a critical understanding of the enzymatic dynamics of the entire repair process was lacking. In an early attempt in 1997, Michel-Beyerle and colleagues (24) used 100-ps temporal resolution to beautifully observe electron injection from the excited cofactor to the substrate. In 2003, MacFarlane & Stanley (25) used 850-fs resolution to clearly show the formation of the repaired thymine product. However, the overall repair dynamics remained unknown, and the entire mechanism still was not determined. For a 6-4PP lesion, several repair mechanisms by photolyase were hypothesized and examined (19, 26–29) but remained elusive because of experimental difficulty and reaction complexity.

In 2005, a major advance involved the direct observation of a cyclic electron transfer (ET) catalytic reaction for CPD repair with femtosecond-resolved spectroscopy (30). In the past 10 years, significant breakthroughs have been reported, and the dynamics of damaged DNA repair by photolyases have been revealed in real time (31–39). We have mapped out the entire dynamic evolution of the repair process from the initial reactants, to various intermediates, and to final products, with more than six elementary steps in the catalytic complex reaction at the most fundamental level. This review summarizes recent discoveries in CPD repair, including the characterization of the initial nonequilibrium electron injection, the sequential dimer splitting, the electron tunneling pathways with intervening adenine mediation, the dynamic synergy for high repair efficiency, and finally the nature of the functional state. For 6-4PP repair, a unique proton-coupled ET mechanism involves an initial photon from blue light, a following electron from the cofactor, and a subsequent proton from the enzyme photolyase to synergistically repair the 6-4PP photolesion (38). Also included are rapid advances in recent quantum mechanical calculations of various repair mechanisms (21, 40–44); as such exciting efforts have also been recently reviewed (45, 46), including a review article published in this journal in 2014 (46), they are not repeated here. Rather, this review focuses on recent significant experimental findings.

## 2. DYNAMICS AND MECHANISMS OF DIMER REPAIR

DNA repair by photolyases can include three photoinduced processes: photoinitiation, photoreduction, and photorepair. The first process involves light harvesting, with the second chromophore acting as an antenna pigment to enhance light absorption, especially under dim-light conditions. The excitation energy is efficiently transferred into the catalytic cofactor. In the second process, the cofactor is photoreduced *in vitro* from neutral semiquinone FADH<sup>•</sup> to anionic hydroquinone FADH<sup>-</sup>. Purification of photolyase under aerobic conditions gives FAD and FADH<sup>•</sup> due to oxygen, and FADH<sup>•</sup> needs to be converted to FADH<sup>-</sup> *in vitro*. The *in vivo* cofactor is in the FADH<sup>-</sup> state (8); thus, the second step is not necessarily occurring in the biological cell because of the low

oxygen concentration (9). The third process involves catalytic repair with the cofactor FADH<sup>-</sup> either by direct excitation with blue light or through resonance energy transfer from the antenna molecule. This section summarizes the dynamics of all three photoinduced processes with an emphasis on the photorepair of biological function.

## 2.1. Photoinitiation and Resonance Energy Transfer

Photolyases contain the second chromophore of either methenyltetrahydrofolate (MTHF) or 8-hydroxy-7,8-didemethyl-5-deazariboflavin (8-HDF) for light harvesting (10, 11), with some also containing flavin mononucleotide (FMN) and FAD as a photoantenna (47, 48). Unlike the nucleotide-like chromophores (e.g., FAD, FMN, and 8-HDF) deeply buried in the N-terminal  $\alpha/\beta$  domain, the photoantenna MTHF is located in a shallow cleft between the  $\alpha$ -helical and  $\alpha/\beta$  domains and partially sticks out at the enzyme's surface (**Figure 2a**). In *Escherichia coli* photolyase,

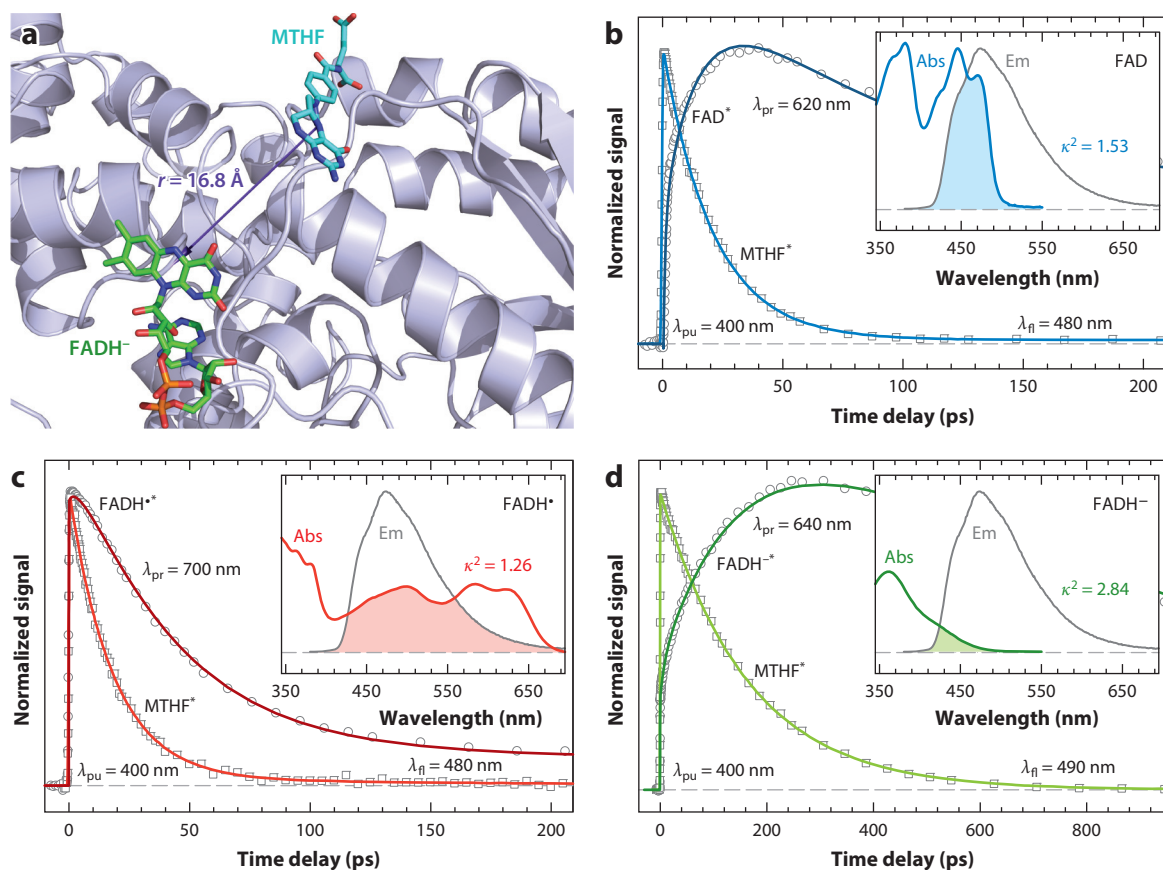


**Figure 2**

(a) X-ray crystal structure of *Escherichia coli* photolyase containing an antenna chromophore, methenyltetrahydrofolate (MTHF; cyan), and a catalytic cofactor (FADH<sup>-</sup>; green) with a center-to-center distance of 16.8 Å. (b–d) Femtosecond fluorescence and absorption transients at three redox states: (b) flavin adenine dinucleotide (FAD), (c) FADH<sup>+</sup>, and (d) FADH<sup>-</sup>. The fluorescence transients ( $\lambda_{fl}$ ) reflect the quenching dynamics of the energy donor MTHF\*, and the absorption signals ( $\lambda_{pr}$ ) mainly reflect the formation and decay dynamics of the energy acceptor FADH<sup>+</sup>. (Insets) The spectral overlaps of the MTHF emission spectrum (Em) with the flavin absorption spectra (Abs) at the three redox states and the orientation factors ( $\kappa^2$ ) from the experimental results.

the distance separation between the antenna MTHF and the cofactor flavin is 16.8 Å, and the mechanism of energy transfer over such a long distance is of the Förster type via a long-range dipole-dipole interaction. MTHF has a much larger extinction coefficient than does FADH<sup>-</sup>, and such energy transfer increases the overall DNA repair efficiency. Early time-resolved studies reported the quenching dynamics of the excited MTHF in photolyase (49–51). However, because of the difficulty in measuring the MTHF lifetime in the binding site of photolyase without the cofactor acceptor, the energy transfer efficiency cannot be accurately calculated and could be erroneously estimated (51). We recently screened mutations at the active site and obtained a N341A mutant of *E. coli* photolyase so that the flavin cofactor is released from the active site but the MTHF in the binding site is not affected. With the accurate determination of the excited MTHF lifetime (2.6 ns), we systematically measured the transfer dynamics in three flavin states of oxidized FAD (20 ps), neutral semiquinone FADH• (18 ps), and fully reduced anionic hydroquinone FADH<sup>-</sup> (170 ps) (**Figure 2b–d**) (52). Not only were the dynamics of the excited donor MTHF characterized, but, more importantly, the product formation of the excited acceptor through the excitation energy transfer from MTHF\* was observed for all three flavin states, confirming the resonance energy transfer mechanism, including the recently proposed intermolecular coulombic decay mechanism (53). The resulting energy transfer efficiency to the functional cofactor FADH<sup>-</sup> is as high as 94%.

All three kinds of energy transfer dynamics follow single exponential behavior, reflecting a relatively rigid configuration of the energy donor and acceptor (the orientation factor,  $\kappa^2$ ) and a constant spectral overlap integral ( $J$ ) (54), indicating the negligible time-resolved fluorescence Stokes shifts of the excited MTHF at the binding site (55). With the determined resonance energy transfer rates and calculated spectral integrals, we obtained  $\kappa^2 = 1.53, 1.26,$  and  $2.84$  for FAD, FADH•, and FADH<sup>-</sup>, respectively (**Figure 2b–d**), and found the optimum structural alignment for the functional state FADH<sup>-</sup> over the course of evolution with the largest orientation factor, although the functional state has the smallest spectral overlap integral (**Figure 2d**). Significantly, the theoretical orientation factors (1.58, 1.29, and 2.23, respectively) from quantum chemical calculations of the donor and acceptor structures and the transition dipole moments agree perfectly with the obtained experimental values (**Figure 2b–d**) (52), further ascertaining the resonance energy transfer mechanism. Similar theoretical studies have reported a large orientation factor of 1.82 for *Anacystis nidulans* photolyase with an 8-HDF antenna chromophore (56), and the X-ray structure gave an estimated value of 1.60 (57). Thus, under physiological conditions, photolyases adopt the optimized orientation of their photopigments to efficiently convert solar energy to repair damaged DNA.

## 2.2. Photoreduction and Intraprotein Electron Transfer

In the past few decades, the photoreduction of FADH• in photolyases has received significant attention (58–62), although this photoinduced process is not biologically relevant in vivo. Such studies are important because we need to understand the mechanism of photoreduction in vitro. Photolyases are also excellent model systems for studying the dynamics of intraprotein ET with multiple electron tunneling pathways and for understanding the initial signaling state induced by electron flow in cryptochromes, which are homologous photoreceptors involved in the synchronization of biological clocks (33, 63–71). Extensive characterizations with various site-directed mutations have identified all possible electron donors in photolyases and determined their ET timescales (**Figure 3**) (60, 62). The excited FADH• behaves as an electron sink to draw electron flow from a series of encircling aromatic molecules from the active site in the center to the protein surface (**Figure 3a**). The dominant electron flow follows the conserved tryptophan triad across the

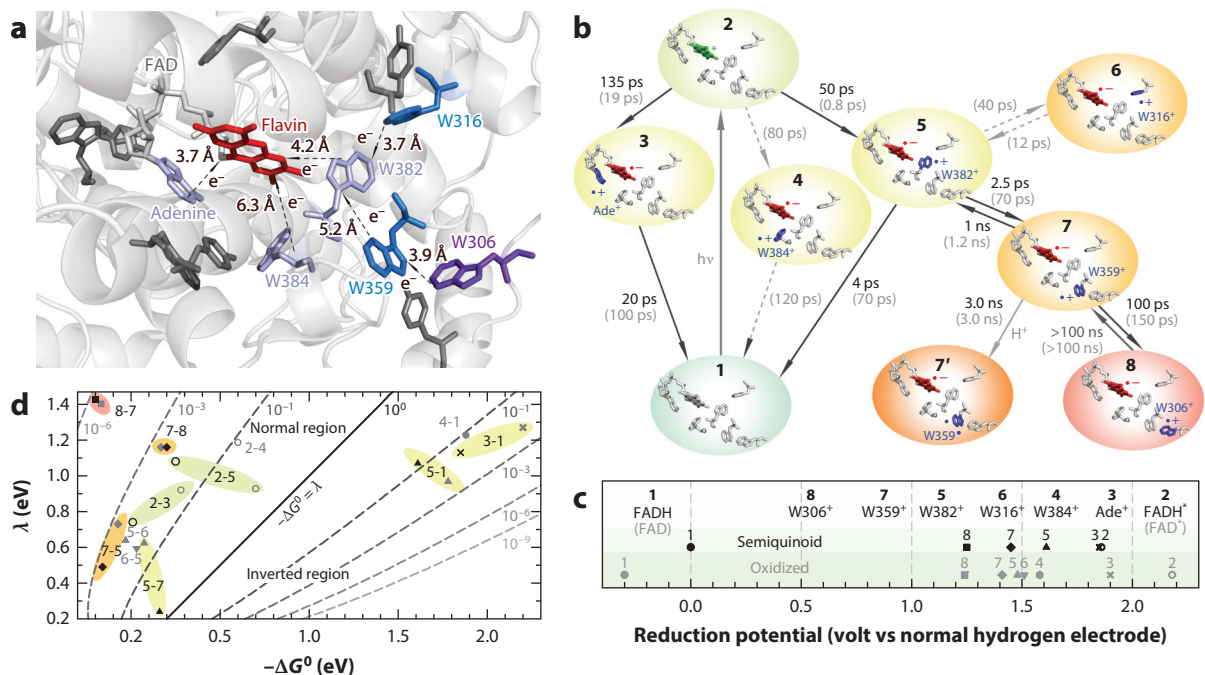


**Figure 3**

(a) Electron transfer (ET) networks in a photolyase with all tunneling distances shown. The flavin moiety of flavin adenine dinucleotide (FAD; red) behaves as an electron sink to draw electron flow from a series of aromatic molecules. The adenine moiety, W384, and W382 (light purple) have direct ET with flavin in the first layer, whereas W316 and W359 (blue) form the second layer, having direct ET with W382. In the third layer, W306 (purple) is exposed to the protein surface. All other aromatic residues of tryptophan and tyrosine (gray) near the ET networks are also shown. (b) Dynamics and timescales of all elementary ET steps for the neutral semiquinoid state (black) and the oxidized state (gray). Note that some ET channels may not be active in the semiquinoid state. (c) The derived reduction potentials of all involved species (black for semiquinone and gray for oxidized). (d) Two-dimensional plot of the Franck-Condon (energy) parts of ET rates relative to the free energy ( $\Delta G^0$ ) and reorganization energy ( $\lambda$ ) for all electron tunneling steps with an electronic coupling constant of  $\beta = 1.4 \text{ \AA}^{-1}$ . The charge-recombination steps with the flavin moiety at both redox states fall in the Marcus inverted ET region ( $-\Delta G^0 > \lambda$ ), and all other ET reactions fall in the Marcus normal region ( $-\Delta G^0 \leq \lambda$ ). The shaded circles group the same ET processes in the two redox states for comparison of their driving forces and reorganization energies.

different layers of donors with multiple tunneling steps. **Figure 3b** also shows the photoreduction of oxidized FAD in *E. coli* photolyase, providing mechanistic insight into the ET dynamics for the photoreceptor (and magnetoreceptor) cryptochrome, a similar chemical and structural motif that exists around the flavin (72–74). We identified 12 elementary ET steps and six ET reaction pairs and derived a series of reduction potentials for the same aromatic residues (**Figure 3c**) and local reorganization energies (**Figure 3d**). These forward ET dynamics occur ultrafast, in less than 150 ps, and the reverse electron flow from the flavin is slow, on the order of nanoseconds, to ensure a high reduction efficiency. The photolyase exhibits a distinct reduction-potential gradient along the same aromatic residues with favorable reorganization energies to drive highly unidirectional electron flow toward the active-site center of FADH<sup>•</sup> or FAD from the protein surface.

All these ET dynamics on the picosecond timescale in photolyases follow stretched exponential behavior and are strongly coupled with local protein and solvent relaxations (33, 34, 38, 75, 76). We have carefully measured the active-site solvation dynamics by following the fluorescence temporal evolution for both CPD and 6-4PP photolyases, and the local relaxations also occur on

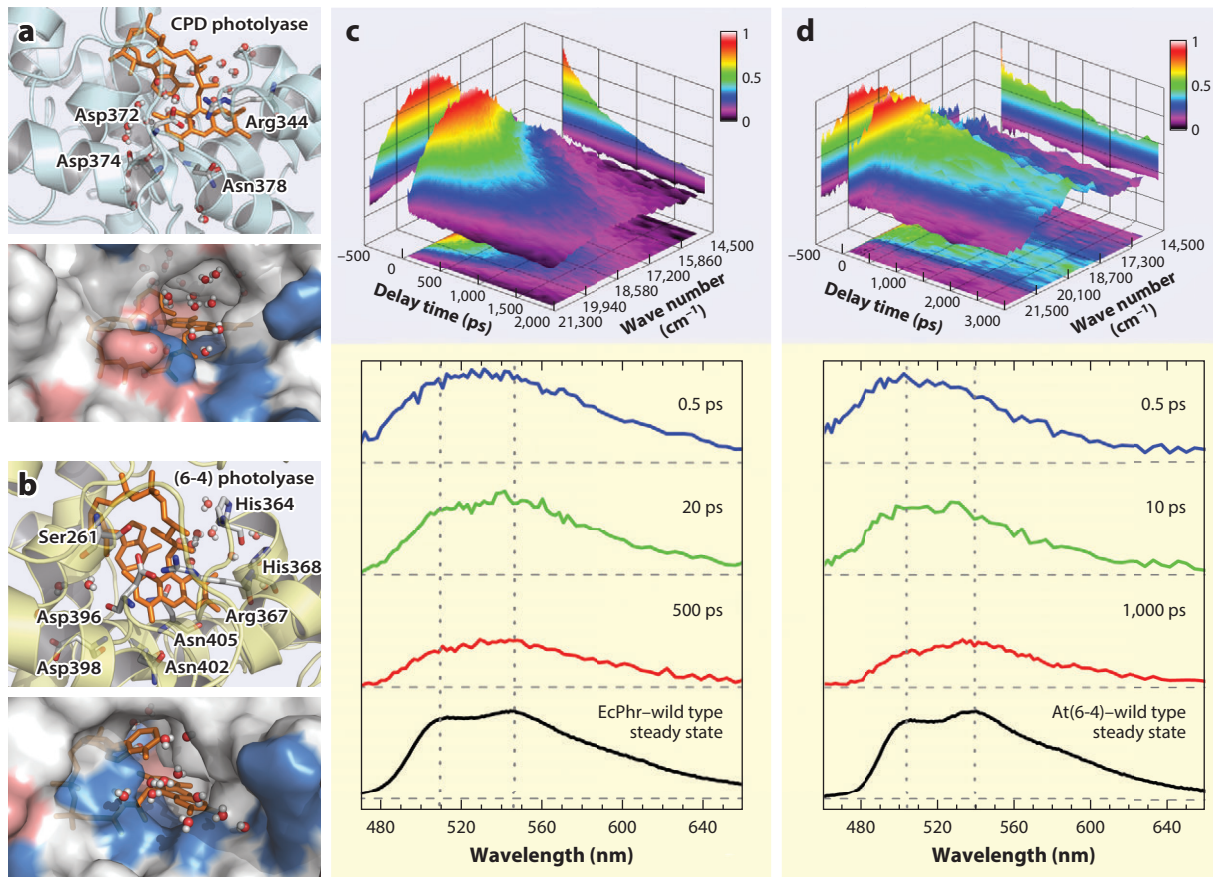


**Figure 4**

(*a,b*, top panels) Close-up view of the flavin active site of (*a*) cyclobutane pyrimidine dimer (CPD) photolyase and (*b*) the (6-4) photolyase with the neighboring polar/charged residues and trapped-water molecules within 8 Å from one snapshot of 1-ns molecular dynamics simulations for each site. (Bottom panels) Corresponding surface maps of the molecular dynamics snapshots, showing the local topography, chemical property [negative charged residue (red) and positive charged residue (blue)], and trapped-water molecules at these sites. (*c,d*, upper panels) Three-dimensional representation of femtosecond-resolved emission spectra of (*c*) *Escherichia coli* photolyase and (*d*) *Arabidopsis thaliana* (6-4) photolyase along time (picosecond) and emission energy (wave number in  $\text{cm}^{-1}$ ) coordinates. The intensity is scaled by the color coding. (Lower panels) Snapshots of femtosecond-resolved spectra at three typical delay times for the two sites with their corresponding steady-state emission spectra. For comparison and clarity, the steady-state emission peaks are marked by the gray dotted lines to show the spectral peak and shape evolutions.

a similar picosecond timescale (**Figure 4**) (55), analogous to the hydration (solvation) dynamics at the surfaces, interfaces, and binding pockets of many proteins (77–82). The derived relaxation correlation functions of the active sites can be represented by multiple exponential decays, from a few to hundreds of picoseconds (55). With the Sumi-Marcus two-dimensional ET theory (75) or other theoretical models (83–85), detailed analyses of ultrafast protein ET provide deep insights into the local reorganization energies (inner versus outer or solute versus solvent) and the coupling (or modulation) of the ET tunneling process with protein fluctuations. Such stretched nonequilibrium behaviors are general to ultrafast dynamical processes occurring in proteins. When the ET dynamics are much faster than local protein fluctuations, single exponential behaviors are observed

again, as demonstrated by the recent observation in flavodoxin (86). The local environment seems to be frozen on the ET time window, and only its electrostatics contributes to the ET dynamics.

### 2.3. Photorepair and Intermolecular Electron Transfer

The enzymatic reaction of UV-damaged DNA repair involves many elementary steps. With femtosecond temporal resolution and single-residue spatial resolution, the entire evolution of the repair processes has been mapped out by probing the dynamics from all initial reactants, to various intermediates, and to the final products. Six elementary processes have been revealed, including three intermolecular ET reactions and two bond-breaking and -making steps. The electron tunneling pathways have been determined, and the high repair efficiency has been evaluated. Only the fully reduced FADH<sup>-</sup>, not other flavin redox forms, as the active state for biological repair function has been elucidated.

**2.3.1. Nonequilibrium electron injection and sequential dimer splitting.** To successfully map the catalytic evolution of CPD repair, researchers first followed the changes of the flavin redox states during the repair reaction (**Figure 5a**) because these flavin species have different absorption in the visible-light region (**Figure 1b**); thus, spectral detection is simpler (30). The thymine-related species of various intermediates and final products have absorption in the UV region. **Figure 5b** shows the stretched nonequilibrium dynamics of electron injection from the excited FADH<sup>-\*</sup> to the substrate CPD in 170 ps with a stretched parameter of 0.71 [with  $Ae^{-(t/\tau)^\beta}$  and the average time calculated by  $(\tau/\beta)\Gamma(1/\beta)$ ] and the electron return from the repaired thymine to the intermediate FADH<sup>•</sup> in 560 ps to restore the active-state FADH<sup>-</sup> and close the entire photocycle. This observation was significant and showed that the entire enzymatic repair occurs ultrafast, in less than 1 ns, and the measured turnover in milliseconds to seconds (87) was actually masked by the recognition process.

It is challenging to identify how the anionic thymine dimer breaks after it accepts one electron. The dimer splitting was completely solved with the use of systematic measurements in the UV region (**Figure 5c**) and knowledge of the overall flavin dynamics (34). The two C5–C5' and C6–C6' bonds are broken sequentially. The C5–C5' bond splits repulsively and ultrafast, in less than a few picoseconds, and the C6–C6' bond cleavage takes place in 90 ps after the energy redistribution in the radical intermediate. We have successfully detected the dynamics of the intermediates T<sup>-</sup>-T<sup>-</sup> after the first C–C cleavage and T<sup>-</sup> after complete dimer splitting and the final product formation

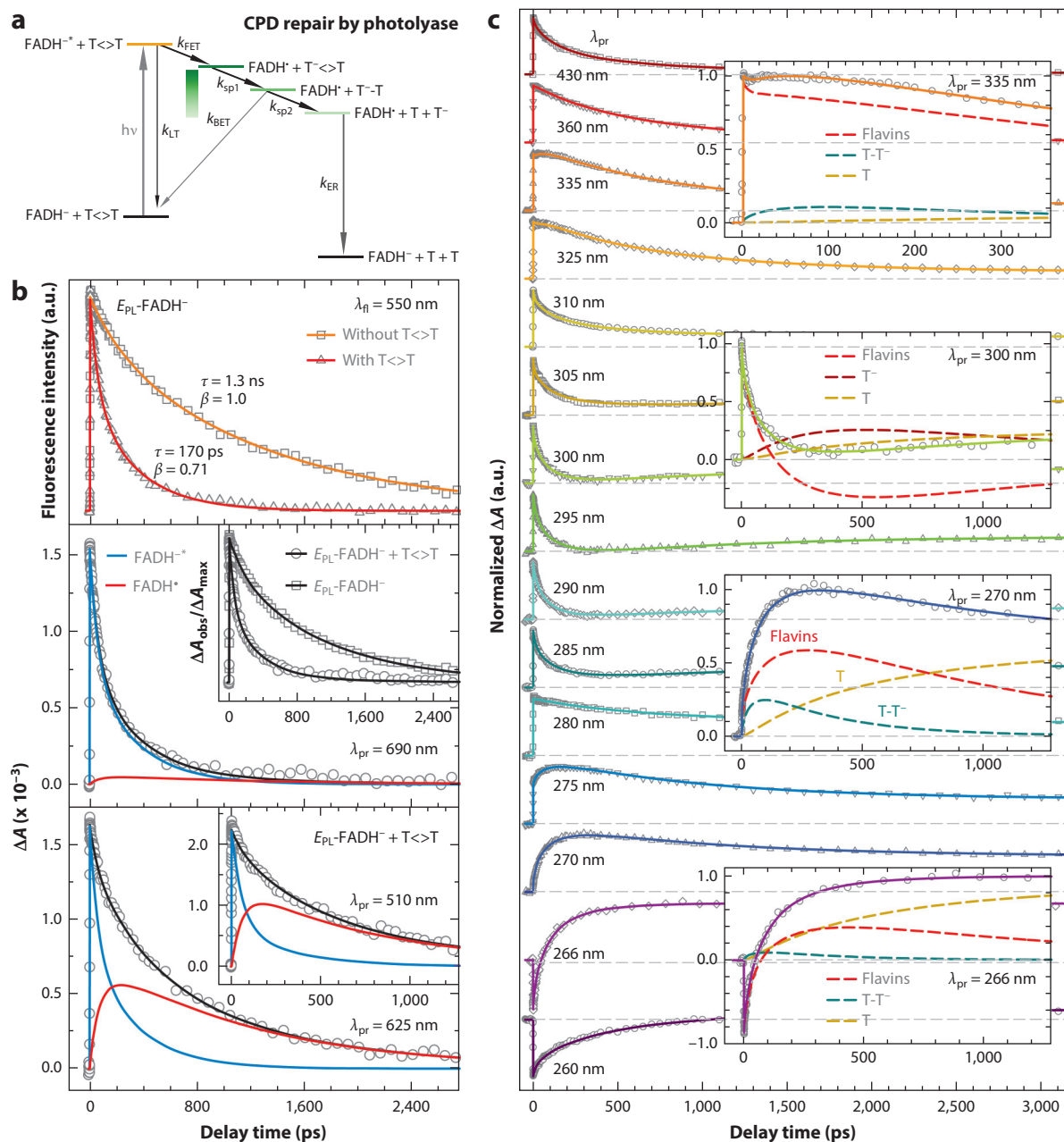
---

#### Figure 5

(a) A sequential scheme of cyclobutane pyrimidine dimer (CPD) repair by photolyases. It includes the forward electron transfer (reaction rate  $k_{\text{FET}}$ ) from FADH<sup>-\*</sup> to the thymine dimer upon light excitation and the repair channel, including the splitting of two bonds of C5–C5' (reaction rate  $k_{\text{sp1}}$ ) and C6–C6' (reaction rate  $k_{\text{sp2}}$ ) in the thymine dimer with subsequent electron return (reaction rate  $k_{\text{ER}}$ ) after complete ring splitting. Two nonrepair bifurcation steps, including the lifetime emission (reaction rate  $k_{\text{LT}}$ ) and futile back electron transfer (reaction rate  $k_{\text{BET}}$ ), are shown as well. (b, top panel) The fluorescence transients at 550 nm, showing the dynamics of FADH<sup>-\*</sup> with and without the substrate thymine dimer. (Middle panel) The absorption transient probed at 690 nm, showing a dominant contribution of FADH<sup>-\*</sup> decay with a minor signal from FADH<sup>•</sup>. The inset shows the drastically different dynamics with and without the CPD substrate. (Bottom panel) Absorption transients probed at 625 and 510 nm showing both FADH<sup>-\*</sup> and the intermediate FADH<sup>•</sup> dynamics. (c) Femtosecond-resolved transient absorption dynamics of reactants, various intermediates, and products probed at the visible and UV regions. (Insets) Transient absorption signals probed at 335, 300, 270, and 266 nm, respectively. These dynamics are systematically fitted by the total flavin-related species (FADH<sup>-\*</sup> + FADH<sup>•</sup> + FADH<sup>-</sup>; dashed red line), thymine dimer intermediate T<sup>-</sup>-T<sup>-</sup> (dashed dark teal line), repaired thymine anion (dashed dark red line), and final thymine products (dashed dark yellow line).

of T after the electron return to the cofactor. Such dynamical splitting processes have been theoretically calculated in a water environment using ab initio molecular dynamics simulations, and similar ultrafast sequential breakage of the two C–C bonds has also been observed (88, 89).

**2.3.2. Repair photocycle and molecular mechanism.** Figure 6 shows the complete photocycle with the local active-site structure. To our knowledge, CPD photolyase is the first enzyme system



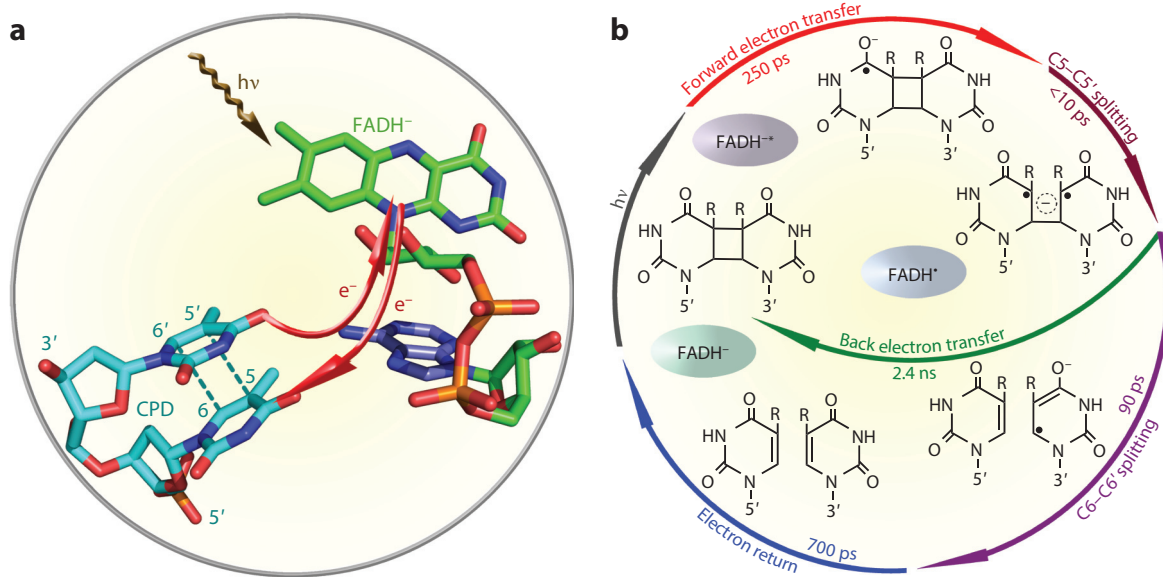


**Figure 6**

(a) A close-up view of the relative positions of the catalytic cofactor FADH<sup>-</sup> and the repaired substrate in *Anacystis nidulans* photolyase with the electron tunneling pathways in repair. (b) Complete photocycle of cyclobutane pyrimidine dimer (CPD) repair by photolyase. All resolved elementary steps of CPD (thymine dimer) repair are shown, illustrating the complete repair photocycle on ultrafast timescales and the elucidated molecular mechanism.

for which the entire catalytic dynamics and functional evolution were mapped out in real time at the most fundamental level. Six elementary reactions in the catalytic repair were completely characterized, and the reaction timescales were determined (30, 34). We observed two consecutive competitions in these elementary steps that make key contributions to the final repair. The first one is the forward ET from the excited cofactor flavin (FADH<sup>-\*</sup>) to the substrate thymine dimer (CPD) in an average time of 250 ps relative to the excited-state deactivation process in 1.3 ns. The second one is the C6–C6' bond splitting in 90 ps relative to the futile back ET without repair in 2.4 ns. The C5–C5' bond splitting dynamics is ultrafast, within a few picoseconds. The electron return, which occurs on average in 700 ps after the dimer repair, restores the initial active-state FADH<sup>-</sup> and finishes the repair photocycle. The photocycle is through a radical ET mechanism with no net change in the redox state of the flavin cofactor. The photorepair machinery of the photolyase utilizes the blue-light photon energy and the released energy from the biotransformation of the substrate to repair the UV-damaged cyclobutane dimer in DNA through a cyclic ET process of the flavin cofactor at the active site.

The free energy profile along the reaction coordinate is shown in **Figure 7**. The four elementary ET reactions are involved in repair. The first forward ET from the excited cofactor to the substrate has a small negative free energy (positive driving force) and is in the Marcus normal region. The intact back ET has a very large negative free energy and is usually in the Marcus inverted region. This step cannot compete with the barrierless downhill C5–C5' bond cleavage; thus, the system dominantly evolves along the C5–C5' splitting pathway. After the C5–C5' bond breakage, the intermediate with the flavin cofactor has a small negative free energy because of the high energy of the neutral ground-state diradical, and thus the back ET is in the Marcus normal region again. After the intermediate passes a small barrier with the C6–C6' bond breakage, the electron return

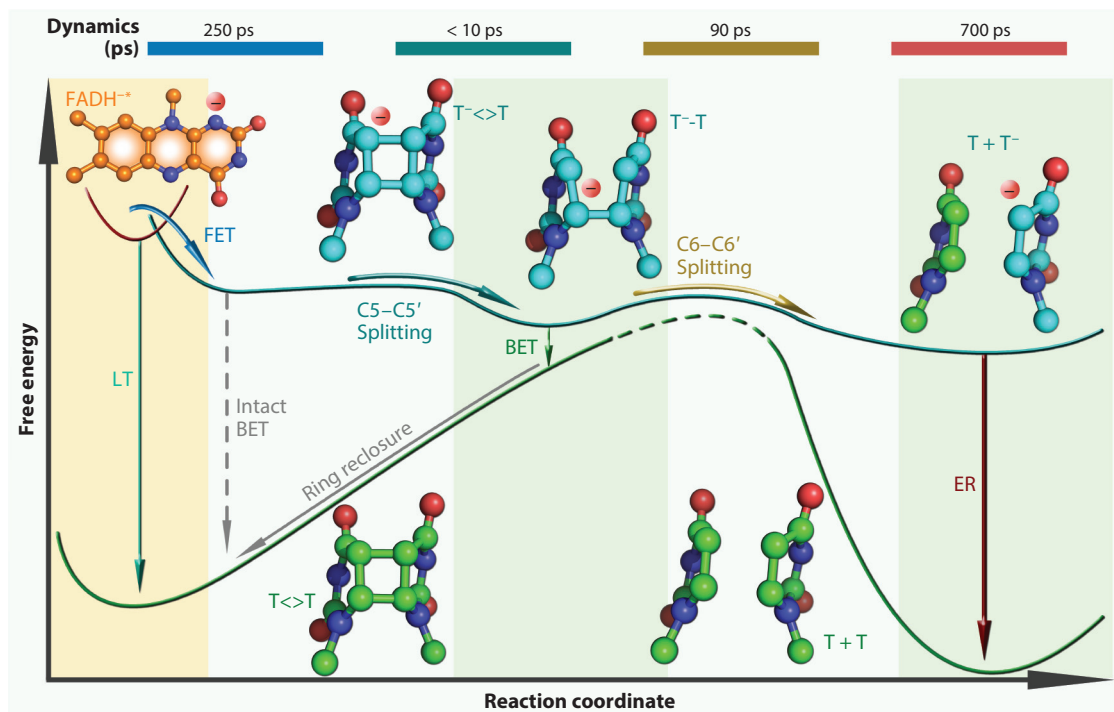


**Figure 7**

Reaction free energy profile along the reaction coordinate for enzymatic DNA repair. Shown are six elementary reaction steps (*solid lines*) with the structures of the excited cofactor flavin (*orange*) and all anionic thymine-related intermediates (*blue*) and products (*green*). The relative energy between each state is mainly determined from recent dynamic measurements. The seventh elementary step of intact back electron transfer (BET) (*dashed line*) is slow and does not occur during repair because of the ultrafast C5–C5' bond splitting. The reaction times are shown at the top of the figure. Abbreviations: ER, electron return; FET, forward electron transfer; LT, lifetime emission.

has a large negative free energy, and the ET is in the Marcus inverted region again. With the determined ET rates, these ET driving forces and related reorganization energies can also be calculated (36).

**2.3.3. Electron tunneling pathways and adenine mediation.** For the three electron reactions of forward ET, back ET, and electron return shown in **Figure 7** between the flavin cofactor and the ground-state thymine dimer, the anionic dimer intermediate, and the anionic repaired thymine, respectively, a central question is how the electron tunnels between the donor and acceptor and whether a specific pathway exists (90–92). Two main tunneling schemes have been proposed based on theoretical calculations (21, 93–95). One model suggests that the electron tunnels through the intervening adenine moiety to the 5' side of DNA at a longer distance of approximately 8 Å, with the unusual U-shape configuration of the cofactor (21, 93). The other model concludes that the electron would travel directly through space to the 3' side of DNA at a shorter distance of 4.3 Å (94, 95). Utilizing the different electron affinities of thymine and uracil, investigators studied the repair dynamics with different dimer substrates, comprising thymine and (deoxy)uracil (U<>T, U<>U, T<>U, and T<>T), and probed the reactants, various intermediates, and final products (**Figure 8a–c**). All the elementary reaction times of the three ET processes and the C6–C6' bond splitting are shown in **Figure 8d**. Clearly, when the uracil moiety is at the distant 5' side of DNA,

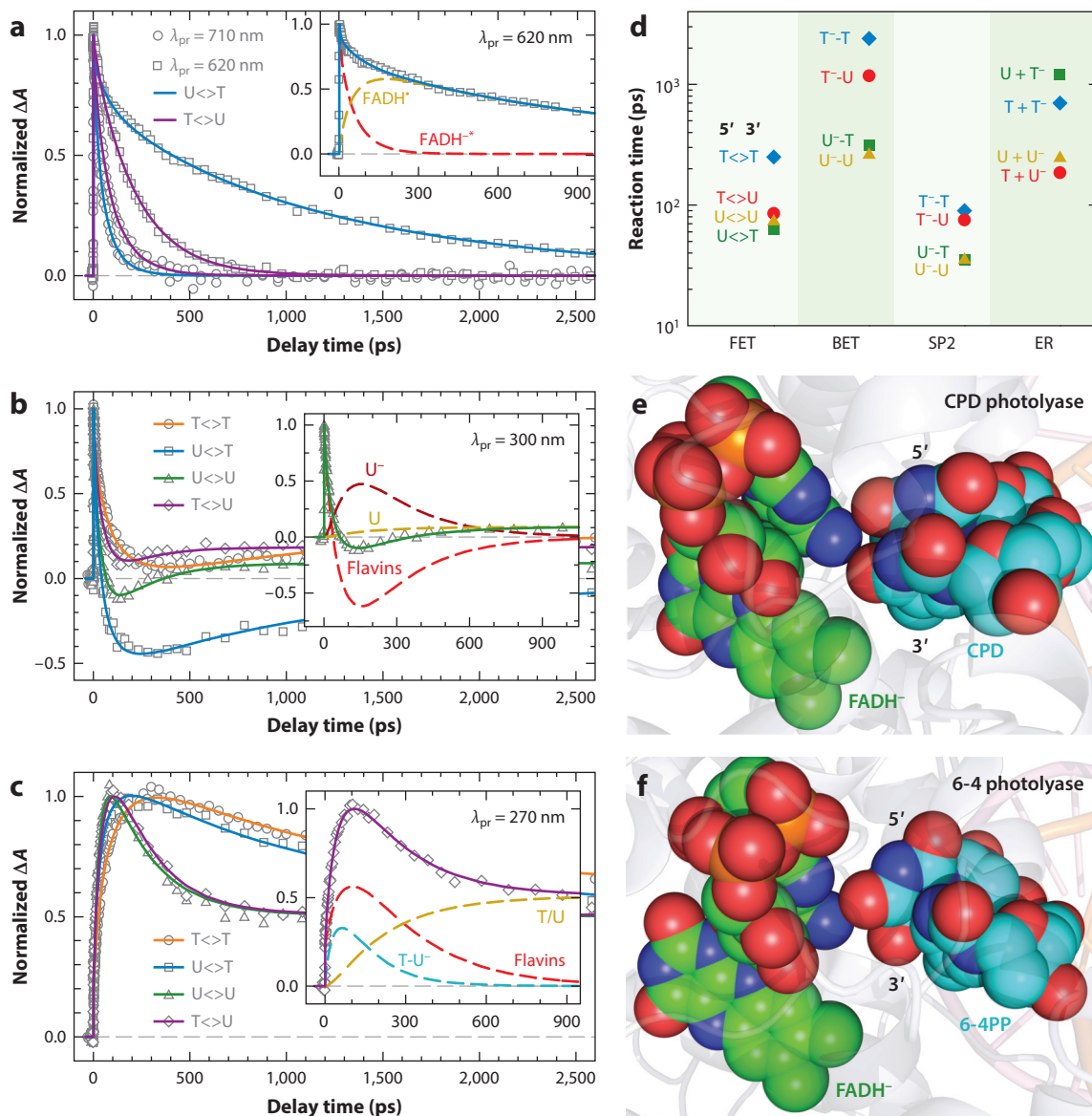


**Figure 8**

(a) Femtosecond-resolved absorption repair signals of two uracil-substituted damaged cyclobutane pyrimidine dimers (CPDs) ( $T \langle \rangle U$  and  $U \langle \rangle T$ ) probed at 710 nm and 620 nm. (Inset) The deconvolution of the repair signal with  $U \langle \rangle T$  probed at 620 nm into  $FADH^{*-}$  and  $FADH^*$ . (b,c) Repair dynamics of  $T \langle \rangle T$  (orange),  $U \langle \rangle T$  (blue),  $U \langle \rangle U$  (green), and  $T \langle \rangle U$  (purple) probed at (b) 300 nm and (c) 270 nm. The insets show the deconvolution of total flavin-related species (dashed red line), anionic CPD intermediates  $T-U^-$  (dashed teal line) and  $U^-$  (dashed dark red line), and the products of T/U (dashed dark yellow line) of repair with  $U \langle \rangle U$  and  $T \langle \rangle U$ . (d) The reaction times of each elementary step observed in the repair of various substrates, including the forward electron transfer (FET), futile back ET (BET), C6–C6' bond splitting, and final electron return (ER) to complete the photocycle. (e,f) The space-filled representation of the relative positions of the active cofactor  $FADH^-$  with the repaired dimer substrate at (e) *Anacystis nidulans* CPD photolyase and (f) the 6-4 photoproduct substrate of *Drosophila melanogaster* 6-4 photolyase. The adenine-mediated tunneling pathways are completely filled with atom contacts, whereas the through-space tunneling routes have gaps in the pathways that cause slower ET owing to weak electronic coupling.

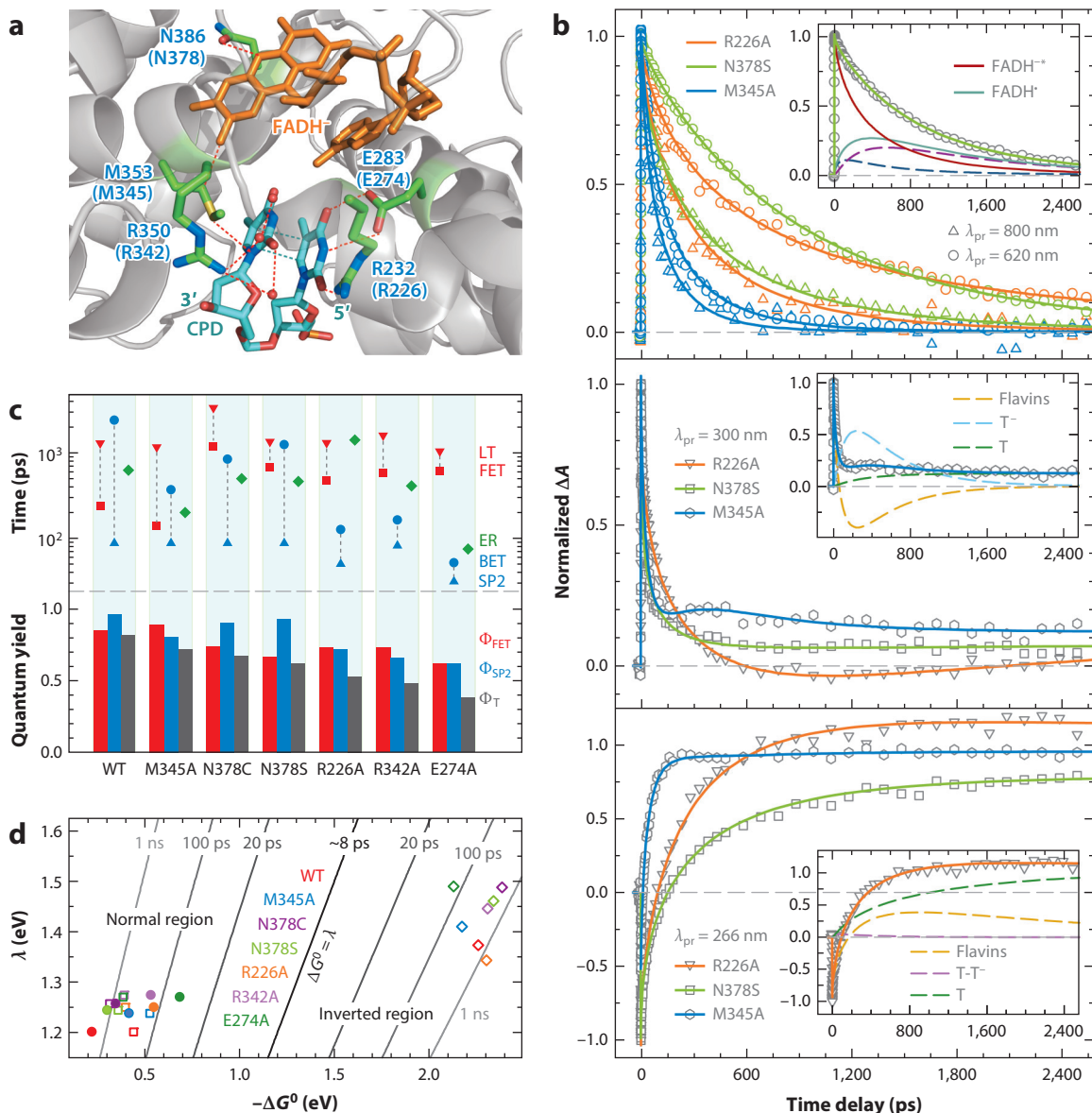
the forward ET is faster, even though  $U \leftrightarrow T$  and  $T \leftrightarrow U$  have a similar reduction potential. Thus, the electron from the excited flavin cofactor tunnels to the 5' side of the damaged DNA through the intervening adenine. After the C5–C5' bond splitting, the intermediates with thymine at the 5' side are stabilized by the methyl group at the C5 position (a tertiary carbon) of thymine, resulting in a smaller driving force and thus slower back ET in the Marcus normal region, whereas the other intermediates with uracil at the 5' side have less stabilization (a secondary carbon at the C5 position) and thus faster ET in the normal region. After repair, the electron return is in the Marcus inverted region, and the dynamics were found to be faster with uracil at the 3' side of DNA; hence, the electron migrates from the 5' to 3' side during dimer splitting owing to a more polar environment around the 3' side that solvates the electron and stabilizes the system.

The tunneling pathway to the 5' side through adenine mediation is further confirmed by the C6–C6' bond splitting time. Similar to the back ET of intermediates discussed above, the stabilization by the methyl group on the tertiary C5 position of thymine at the 5' side results in a longer C6–C6' bond cleavage time (90 ps), whereas the uracil intermediate without the stabilization (a secondary carbon at the C5 position) splits in 35 ps (**Figure 8d**), which is almost three times faster than the thymine intermediate cleavage, demonstrating that the electron ends on the 5' side. **Figure 8e** shows that the local structure and atoms along the adenine-mediated tunneling pathway are all at van der Waals contacts. Further evidence is provided by the forward ET in 6-4PP repair. Both CPD and 6-4PP photolyases have a similar structural motif for the adenine-mediated tunneling pathway to the 5' side (**Figure 8e,f**), and the forward ET dynamics in 6-4PP repair occurs with a similar average reaction time of 280 ps (also see Section 3). The distance separation of the flavin cofactor to the 3' side of damaged DNA in 6-4PP is more than 6.3 Å, and forward ET would take nanoseconds to reach the 3' side. Thus, both photolyases use the same strategy to utilize the critical intervening adenine moiety of the unusual bent configuration of the cofactor flavin to inject one electron through a superexchange mechanism to initiate damaged DNA repair. A recent quantum mechanical calculation reported a similar mechanism but involved the adenine moiety and five water molecules for the electron to tunnel through an adenine-mediated proton wire to reach the 5' side (96).

**2.3.4. Dynamic synergy and high repair efficiency.** The overall repair efficiency of a wild-type *E. coli* photolyase is as high as 0.82 (97). The entire repair process contains at least seven elementary reactions with two competitive bifurcations (**Figure 7**). The first branching is the forward ET against the deactivation process, leading to a quantum yield  $\Phi_{\text{FET}}$  of 0.85. The second branching is the C6–C6' bond splitting competing with the futile back ET without repair, resulting in a quantum yield  $\Phi_{\text{SP2}}$  of 0.96. The overall repair efficiency ( $\Phi_{\text{T}}$ ) is the product of the two quantum yields. The central question is how the enzyme optimizes those elementary steps at the active site to reach the maximum repair efficiency. Investigators have studied five critical residues (N378, M345, E274, R266, and R342) having hydrogen bonds with the cofactor or substrate at the active site (**Figure 9a**) by using site-directed mutagenesis (39). N378 was mutated to serine or cysteine, and the other four residues were mutated one at a time using an alanine scan. Similar to the studies of the wild type (Section 2.3.1) and different substrates (Section 2.3.3), the repair dynamics of each mutant were completely mapped out in real time (**Figure 9b**), and the reaction times of the five elementary steps are shown in **Figure 9c**, along with the corresponding two branching ratios and the overall repair quantum yields from the steady-state measurements. All mutations led to a lower repair quantum yield than that of the wild type. All mutations also altered the reduction potentials of either the flavin cofactor or the substrate and also the local reorganization energies (**Figure 9d**), resulting in the modulations of all three ET dynamics. For the mutations around the

substrate, the C6–C6' bond cleavage time was also varied by different stabilizations of the splitting transition state.

Thus, to maximize the repair efficiency, the wild-type enzyme possesses an active site that is relatively rigid, both structurally and electrostatically, to avoid the ultrafast deactivation of the excited cofactor from the butterfly bending motion (98–100) and to lengthen the excited-state lifetime (98). It has a favorable redox environment that leads to an appropriate FET, not so slow that it results in a lower  $\Phi_{\text{FET}}$  and not so fast that it causes rapid back ET that leads to a lower  $\Phi_{\text{SP2}}$ . After charge separation, the reaction evolves along the trajectory of ultrafast downhill C5–C5' bond splitting and thus eliminates the first intact charge-recombination channel



without dimer splitting. After C5–C5' bond breaking, the reaction encounters a small barrier for the C6–C6' bond splitting, and the reaction bifurcates. The second charge-recombination channel that leads to the reclosure of the dimer ring competes with productive C6–C6' bond cleavage and results in loss of the repair yield. The redox property at the active site is optimized to synergistically balance the FET and BET processes relative to the excited-state deactivation and the dimer splitting, respectively, to achieve the maximum outcome. After the complete dimer splitting, the third charge-recombination channel, an electron return to restore the active flavin cofactor and complete the repair photocycle, should not be too slow in order to avoid any new damage of the repaired DNA by the extra electron (101). Thus, as shown here, any mutation modulates the active-site reduction potentials and ET reorganization energies but always breaks the dedicated synergy of the four main elementary reactions in two competitions, leading to low repair efficiency. Such dynamical synergy is essential and is also the key reason why the enduring biomimetic syntheses gave the best chemical system with the highest repair efficiency of only less than 0.4 (102–104).

**2.3.5. Electron shuttling and functional state.** Photolyases adopt the anionic hydroquinone  $\text{FADH}^-$  as the functional state in vivo, an unusual redox state in flavoenzymes, with a unique bent configuration at the active site. In principle, the substrate thymine dimer can accept one electron to be reduced or donate one electron to be oxidized, and then the ionic dimer subsequently splits into two bases (105, 106). The flavin cofactor has two anionic states of semiquinone  $\text{FAD}^{\bullet-}$  and hydroquinone  $\text{FADH}^-$  that could donate one electron to the substrate and two neutral states of oxidized FAD and semiquinone  $\text{FADH}^\bullet$  that can accept one electron from the substrate. For the anionic flavin, the critical question is why photolyases utilize  $\text{FADH}^-$ , not  $\text{FAD}^{\bullet-}$ , as the active state. For the neutral state, the excited flavin reacts with the neighboring aromatic residues (tryptophan or tyrosine) through ET (see Section 2.2) to obtain one electron and is reduced on the ultrafast timescale (60, 62, 63). One challenging question is whether the neutral flavins can accept one electron from the substrate if the active site becomes inert by mutations of aromatic residues.

For the two anionic states, cyclic ET dynamics between the isoalloxazine ring and adenine moiety were observed, and the adenine behaves as an electron acceptor (**Figure 10a–c**). For  $\text{FAD}^{\bullet-}$ , the forward ET takes 12 ps, and the back ET is even faster, in 2 ps. But for  $\text{FADH}^-$ , the forward ET is slow (in 2 ns), and the back ET is much faster (in 25 ps). Thus, the electron in

### Figure 9

(a) The local structure at the active site of the cyclobutane pyrimidine dimer (CPD) *Anacystis nidulans* photolyase with five critical residues (green), the cofactor flavin (orange), and the thymine dimer substrate (blue). The residues in brackets are for *Escherichia coli* photolyase. (b) Transient absorption signals of three mutants (R226A, N378S, and M345A) probed by a wide range of wavelengths, from the visible to UV region, at 400-nm excitation. (Top panel) Absorption transients probed at 800 nm for the detection of the excited-state flavin ( $\text{FADH}^{\bullet-}$ ) and at 620 nm mainly for the intermediate flavin ( $\text{FADH}^\bullet$ ). Shown in the inset is the deconvolution of the  $\text{FADH}^{\bullet-}$  and  $\text{FADH}^\bullet$  contributions of the N378S mutant, with the latter from two channels (dashed lines). (Middle and bottom panels) Absorption signals probed at 300 nm and 266 nm with distinct dynamic patterns for each mutant. The insets show the deconvolution of the transient signals with the detection of initial reactants, subsequent intermediates, and final products for (middle panel) M345A and (bottom panel) R226A. (c, upper panel) The reaction times for five elementary reactions involved in repair: the deactivation lifetime (LT), forward electron transfer (FET), back electron transfer (BET), the second C6–C6' bond splitting (SP2), and electron return (ER) after repair. The C5–C5' bond splitting is ultrafast for all mutants, within 10 ps, and is not shown here. The dashed lines link two sets of competing channels responsible for the repair efficiency. (Bottom panel) The corresponding quantum yields of  $\Phi_{\text{FET}}$  and  $\Phi_{\text{SP2}}$  for the two sets of competing channels and the resulting total quantum yield of  $\Phi_{\text{T}}$  ( $\Phi_{\text{FET}} \times \Phi_{\text{SP2}}$ ). (d) Two-dimensional contour plot of the ET dynamics relative to the free energy ( $\Delta G^0$ ) and reorganization energy ( $\lambda$ ) for FET (filled circles), BET (open squares), and ER (open diamonds). The first two are in the ET normal region, and the last one is in the inverted region.

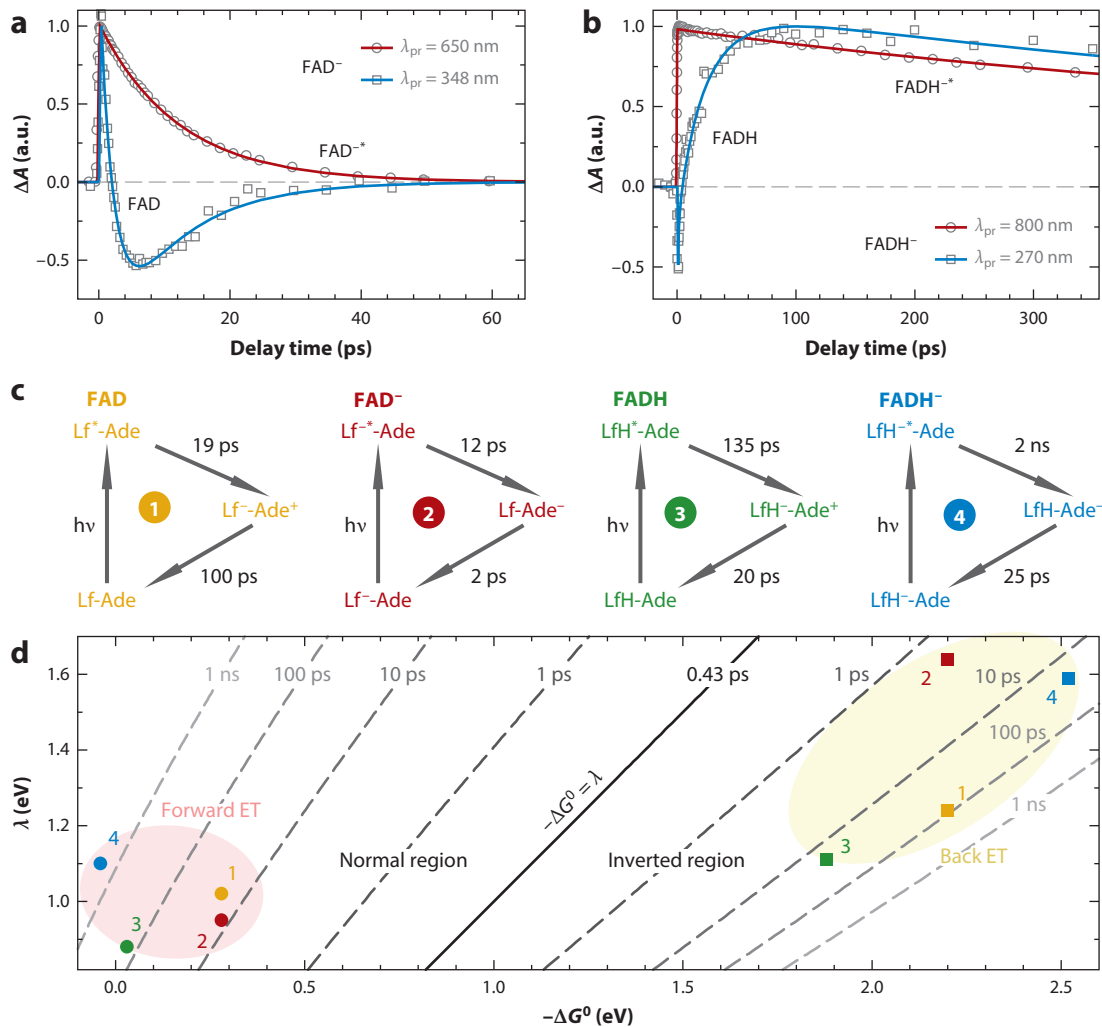


**Figure 10**

(a) Femtosecond-resolved absorption signals of a photolyase at the FAD $\bullet^-$  redox state. The transient at 650 nm shows the dynamics of FAD $\bullet^-$ , and the transient at 348 nm mainly reflects the intermediate signal of FAD by intramolecular electron transfer (ET). (b) Femtosecond-resolved absorption signals of a photolyase at the FADH $\bullet^-$  redox state. The transient at 800 nm shows the dynamics of FADH $\bullet^-$ , and the transient at 270 nm mainly reflects the intermediate signal of FADH $\bullet$  by intramolecular ET. (c) Reaction times and mechanisms of cyclic ET between the lumiflavin (Lf) and adenine (Ade) moieties of the flavin cofactor in all four redox states. For clarity, all dot symbols ( $\bullet$ ) representing radicals have been removed. (d) Two-dimensional contour plot of the ET times relative to the free energy ( $\Delta G^0$ ) and reorganization energy ( $\lambda$ ) for all electron tunneling steps. All forward ET reactions are in the Marcus normal region ( $-\Delta G^0 \leq \lambda$ ), whereas all back ET steps are in the Marcus inverted region ( $-\Delta G^0 > \lambda$ ).

FADH $\bullet^-$  can tunnel further to the substrate in 250 ps, not to the adenine in 2 ns, but in FAD $\bullet^-$ , the electron quickly shuttles between the isoalloxazine ring and adenine moiety within 12 ps, eliminating further tunneling to the substrate. Thus, as the electron donor, the active state of the cofactor flavin has to be FADH $\bullet^-$ , and only FADH $\bullet^-$  can function as the active state. For neutral flavins in an inert environment, the cyclic ET dynamics between the isoalloxazine ring and adenine moiety still occur on the picosecond timescale, but the adenine acts as an electron donor

(**Figure 10c**). For FAD and FADH<sup>•</sup>, the electron shuttles within 100 and 135 ps, respectively, preventing further tunneling from the substrate. **Figure 10d** shows the reorganization energies of these four cyclic ET reactions. Thus, the intramolecular ET dynamics in the four redox states with the bent cofactor configuration reveal the molecular origin of the active state in photolyases. To repair damaged DNA in photolyases, the ET must be from the anionic flavin cofactor, and the intramolecular ET dynamics unambiguously reveal only FADH<sup>-</sup> as the active state rather than FAD<sup>•-</sup> because of the intrinsically slower ET (2 ns) in the former and the faster ET in the latter (12 ps), allowing a feasible, relatively fast, ET (250 ps) to the damaged DNA substrate from FADH<sup>-</sup>, with the intervening adenine moiety in the middle to mediate such initial electron tunneling for repair (37).

### 3. DYNAMICS AND MECHANISMS OF 6-4 PHOTOLESION REPAIR

Understanding 6-4PP repair had been elusive because of the experimental difficulty of substrate synthesis and enzyme instability and the complexity of repair. Recent significant efforts have been made, including the X-ray structure (19) and femtosecond-resolved dynamical studies (38). A major discovery was that the initial ET induced proton transfer from the nearby amino acid histidine to the 6-4PP substrate, and the repair mechanism involved cyclic proton-coupled ET (38). Overall, the initial electron transfer, similar to that in CPD repair, tunnels along the adenine-mediated pathway to the 5' side of DNA in 225 ps with a stretched parameter of 0.8 (**Figure 11a**). After charge separation, the reaction bifurcates: One pathway is the futile back ET to the original state without repair, in 50 ps, with a branching of 0.9, and the other one proceeds to proton transfer with the histidine in 425 ps, with a branching of 0.1, as shown in **Figure 11b** by the detection of both the dynamics and the population ratio of the radical intermediate FADH<sup>•</sup>. A series of mutations of the histidine to other residues at the active site results in the complete loss of repair owing to the lack of a proton donor. Cyclic ET still occurs without any repair, as shown in **Figure 11c,d** by the complete return of the FADH<sup>•</sup> signal to zero. Proton transfer was further confirmed by the reaction in deuterium water; the transfer slows down because of heavy D<sup>+</sup> transfer from the deuterated histidine, and the resulting repair branching decreases to 0.05, also shown in **Figure 11c,d** by the FADH<sup>•</sup> signal. The 6-4PP intermediate was also observed (**Figure 11d**). However, many reaction details and related intermediates, especially after the proton transfer, need to be examined further. On the theoretical side, significant efforts have recently been made and various repair models have been proposed to explain the complicated repair process (41–44); even a two-photon repair mechanism was proposed (43), and an experimental observation was recently claimed (107). Our observations favor the one-photon repair process, and such a two-photon repair process seems unlikely.

A catalytic photocycle for the repair of the thymine (6-4) photoproduct based on these recent findings is given in **Figure 12**. In this scheme (**Figure 12b**), the primary reactions are the initial ET (I to II) and the subsequent proton transfers (II to III). The ET-induced proton transfer from a histidine residue in photolyase to the 6-4PP is a key step in the repair photocycle, acting similar to the dividing line in the transition state and making the subsequent reactions downhill, without the possibility of back reaction. This critical step competes with the back ET, resulting in an overall repair quantum yield of ~0.1, which is probably the maximum value that could be achieved, for such a structurally and chemically challenging reaction, through slowing down the back ET and speeding up the proton transfer process. The successive elementary steps naturally proceed to an intramolecular proton transfer from the –OH group on C5 of the 5' base to N3 at the 3' base (108) to form a transient zwitterion and then the oxygen atom attack of the C4 position at the 3' base to form a transient oxetane-type structure (III). A transient H<sub>2</sub>O formation model

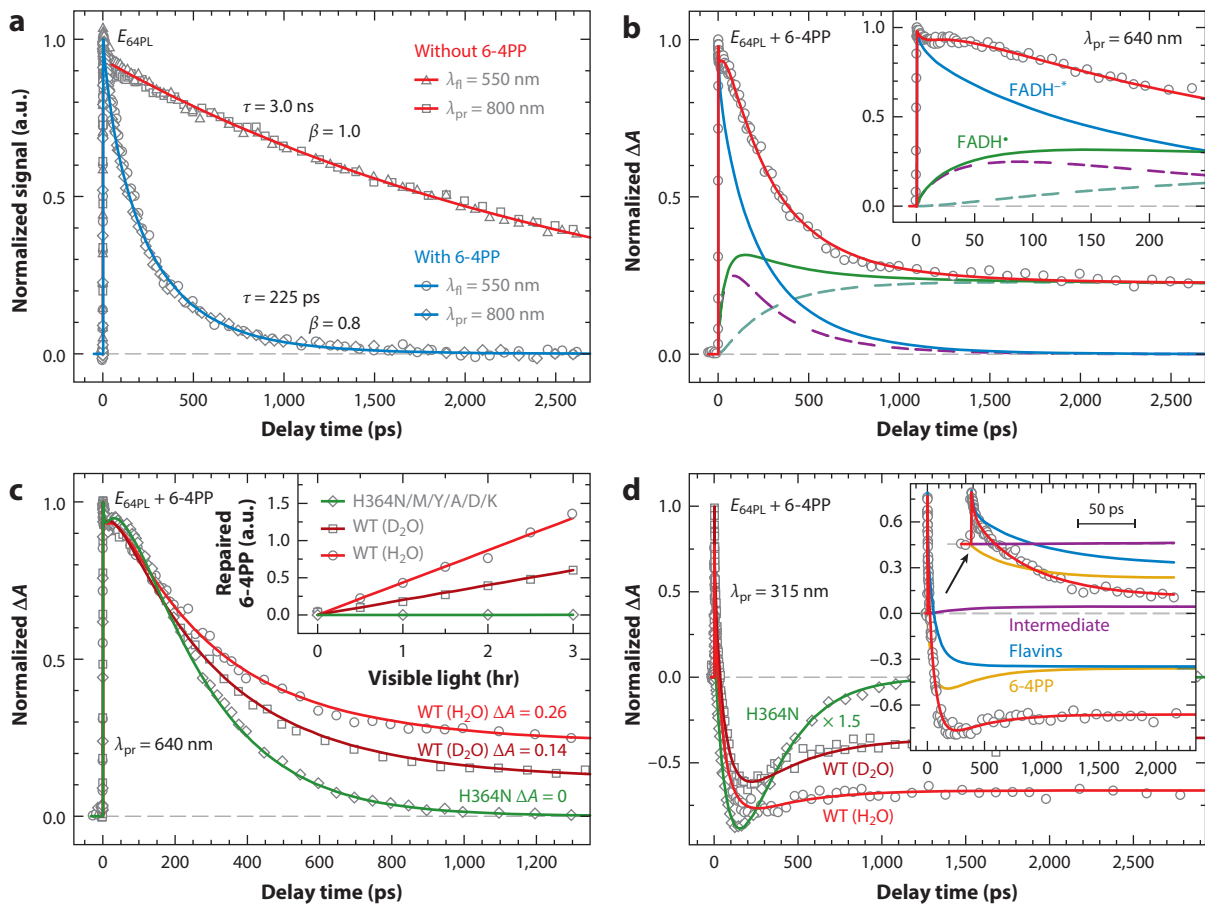


**Figure 11**

Femtosecond-resolved dynamics of flavin species involved in the repair of damaged DNA by a (6-4) photolyase enzyme. (a) Normalized signals detected by both fluorescence (gated around the emission peak of 550 nm) and absorption (probed at 800 nm) methods without (red) and with (blue) the substrate in the active site, showing the same lifetime and forward electron transfer decays. (b) Transient absorption signal probed at 640 nm with both FADH<sup>-•</sup> (blue) and FADH<sup>•</sup> (green) detection. The total FADH<sup>•</sup> signal is from the two contributions of the initially formed FADH<sup>•</sup> signal and the branched FADH<sup>•</sup> signal in the repair channel. (Inset) The flat signal in tens of picoseconds, reflecting an apparent fast rise signal. (c) Transient absorption signals probed at 640 nm of the H364N mutant in H<sub>2</sub>O (green line) and wild-type (WT) enzymes in D<sub>2</sub>O (dark red line) compared with the WT in H<sub>2</sub>O (light red line). The corresponding relative steady-state quantum yield measurements are shown in the inset. (d) Transient absorption signals probed at 315 nm from the WT, including three contributions of overall flavin species (blue line), 6-4PP (yellow line), and a captured intermediate (purple line), shown in the inset. The H364N mutant signals decay to zero with a futile electron transfer cycle.

that was previously prevalent (19, 109), which proposes direct breakage of the C–O bond at the 5' base after the initial proton transfer, seems unlikely because it necessitates a series of proton transfer reactions, including the protonation of the carbonyl group at the 3' base, but there are no potential proton donors in the proximity of this carbonyl group. In addition, any interruption in such a complicated scheme proposed by the H<sub>2</sub>O model would be expected to give rise to damaged DNA at a significant rate, which is not observed in the repair reaction by (6-4) photolyase (26, 27). In contrast, the scheme emerging from our studies in which the simple transient oxetane

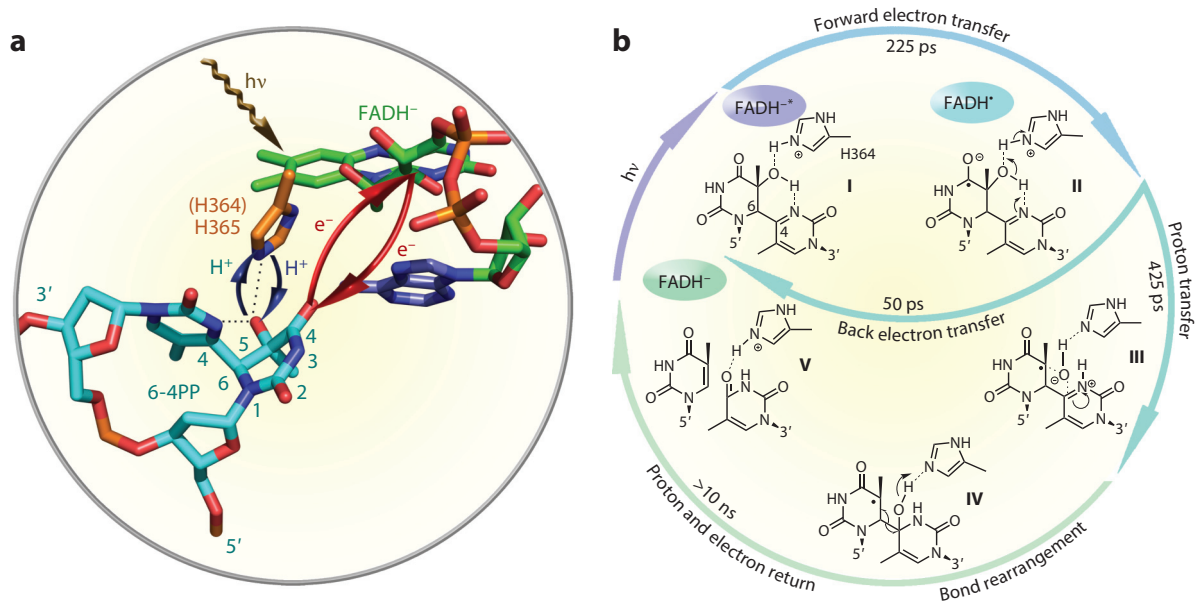


**Figure 12**

(a) A close-up view showing the relative positions of the catalytic cofactor FADH<sup>-</sup>, the conserved histidine residue, and the pyrimidine-pyrimidone (6-4) photoproduct (6-4PP) substrate [H364 in *Arabidopsis thaliana* and H365 in *Drosophila melanogaster* (6-4) photolyase]. (b) The repair photocycle of 6-4PP by (6-4) photolyase. The resolved elementary steps include forward electron transfer in 225 ps (I to II), back electron transfer in 50 ps without any repair (II to I), and parallel, catalytic proton transfer between the enzyme (H364) and the substrate (II to III), induced by the initial electron transfer, in 425 ps. This proton transfer is the determinant step in repair and determines the overall repair quantum yield. The subsequent repair reactions involve a series of atom arrangements with bond breaking and making (III to IV), and final proton and electron returns (to the H364 residue and flavin cofactor, respectively) to convert the 6-4PP to two thymine bases on timescales longer than 10 ns (IV to V).

formation facilitates oxygen atom transfer from the 5' to 3' base followed by C6–C4 bond splitting (IV) would be less prone to a mutagenic side reaction. In this scheme, following an oxygen atom transfer and C–C bond cleavage, the proton returns to the essential histidine residue and the electron returns to FADH<sup>\*</sup> to restore the enzyme to its active form and the 6-4PP to two thymine bases (V).

#### 4. CONCLUDING REMARKS

This review summarizes the experimental advances made in the past decade on our understanding of the fascinating photorepair machinery, photolyases, for restoring two major forms of UV-induced DNA damage, CPD and 6-4PP. With femtosecond temporal resolution and site-directed mutagenesis, we can completely map out the entire enzymatic evolution in real time from the initial reactants, to various intermediates, and to the final products; thus, we can reveal the molecular mechanisms and repair photocycles at the most fundamental level. For the dimer repair, there are six elementary reactions, including three ET steps and two bond-breaking and -making processes in the catalytic process, and all actual reaction times have been determined. A unique electron tunneling pathway has been identified in photolyases with intervening adenine mediation, along with the critical residues at the active site in modulating the repair function, revealing the dynamic

synergy between the elementary reactions in optimizing the repair efficiency, and the nature of the functional state. To our knowledge, photolyases are the first enzyme system in which the entire catalytic evolution is completely characterized in real time, with each elementary step determined with the actual reaction time. For 6-4 photoproduct repair, there is a cyclic proton-coupled ET mechanism, and such challenging repair requires three particles (a photon, an electron, and a proton) to synergistically reverse the peculiar 6-4 photodamage. More studies are needed to resolve the details for a complete understanding of the entire repair process. The elucidation of two repair photocycles is significant and provides a molecular basis for practical applications (110), such as for the rational design of drugs to cure skin cancer. By integrating femtosecond spectroscopy and molecular biology, we can now tackle more complex biological systems, especially photomachinery in nature, and reveal biological dynamics and mechanisms in unprecedented detail.

## DISCLOSURE STATEMENT

The author is not aware of any affiliations, memberships, funding, or financial holdings that might be perceived as affecting the objectivity of this review.

## ACKNOWLEDGMENTS

I thank my longtime collaborator Prof. Aziz Sancar (University of North Carolina) for his help and many fruitful discussions. Owing to space limitations, I apologize to those whose work I was unable to cover in this review. I gratefully acknowledge the generous support initially by the Packard Foundation fellowship and then subsequently by the National Institute of Health (GM074813). I thank all members in my group, both past and present, and those whose efforts, expressed in the publications cited, made the story told here possible. I especially thank Dr. Zheyun Liu for his help in the preparation of the figures and references.

## LITERATURE CITED

1. Johns HE, Pearson ML, Leblanc JC, Helleiner CW. 1964. The ultraviolet photochemistry of thymidylyl-(3'-5')-thymidine. *J. Mol. Biol.* 9:503-24
2. Taylor JS. 1994. Unraveling the molecular pathway from sunlight to skin cancer. *Acc. Chem. Res.* 27:76-82
3. Mitchell DL. 1988. The relative cytotoxicity of (6-4) photoproducts and cyclobutane dimers in mammalian cells. *Photochem. Photobiol.* 48:51-57
4. Brash DE. 1997. Sunlight and the onset of skin cancer. *Trends Genet.* 13:410-14
5. Dulbecco R. 1949. Reactivation of ultra-violet-inactivated bacteriophage by visible light. *Nature* 163:949-50
6. Todo T, Takemori H, Ryo H, Ihara M, Matsunaga T, et al. 1993. A new photoreactivating enzyme that specifically repairs ultraviolet light-induced (6-4) photoproducts. *Nature* 361:371-74
7. Sancar A. 2003. Structure and function of DNA photolyase and cryptochrome blue-light photoreceptors. *Chem. Rev.* 103:2203-37
8. Kim ST, Sancar A, Essenmacher C, Babcock GT. 1993. Time-resolved EPR studies with DNA photolyase: excited-state FADH\* abstracts an electron from Trp-306 to generate FADH<sup>-</sup>, the catalytically active form of the cofactor. *Proc. Natl. Acad. Sci. USA* 90:8023-27
9. Kavakli IH, Sancar A. 2004. Analysis of the role of intraprotein electron transfer in photoreactivation by DNA photolyase in vivo. *Biochemistry* 43:15103-10
10. Selby CP, Sancar A. 2012. The second chromophore in *Drosophila* photolyase/cryptochrome family photoreceptors. *Biochemistry* 51:167-71
11. Kiontke S, Gnau P, Haselsberger R, Batschauer A, Essen LO. 2014. Structural and evolutionary aspects of antenna chromophore usage by class II photolyases. *J. Biol. Chem.* 289:19659-69

12. Essen LO. 2006. Photolyases and cryptochromes: common mechanisms of DNA repair and light-driven signaling? *Curr. Opin. Struct. Biol.* 16:51–59
13. Brettel K, Byrdin M. 2010. Reaction mechanisms of DNA photolyase. *Curr. Opin. Struct. Biol.* 20:693–701
14. Mees A, Klar T, Gnau P, Hennecke U, Eker APM, et al. 2004. Crystal structure of a photolyase bound to a CPD-like DNA lesion after in situ repair. *Science* 306:1789–93
15. Kiontke S, Geisselbrecht Y, Pokorny R, Carell T, Batschauer A, et al. 2011. Crystal structures of an archaeal class II DNA photolyase and its complex with UV-damaged duplex DNA. *EMBO J.* 30:4437–49
16. Hitomi K, Arvai AS, Yamamoto J, Hitomi C, Teranishi M, et al. 2012. Eukaryotic class II cyclobutane pyrimidine dimer photolyase structure reveals basis for improved ultraviolet tolerance in plants. *J. Biol. Chem.* 287:12060–69
17. Pokorny R, Klar T, Hennecke U, Carell T, Batschauer A, et al. 2008. Recognition and repair of UV lesions in loop structures of duplex DNA by DASH-type cryptochrome. *Proc. Natl. Acad. Sci. USA* 105:21023–27
18. Glas AF, Maul MJ, Cryle M, Barends TRM, Schneider S, et al. 2009. The archaeal cofactor F<sub>0</sub> is a light-harvesting antenna chromophore in eukaryotes. *Proc. Natl. Acad. Sci. USA* 106:11540–45
19. Maul MJ, Barends TRM, Glas AF, Cryle MJ, Domratcheva T, et al. 2008. Crystal structure and mechanism of a DNA (6-4) photolyase. *Angew. Chem. Int. Ed. Engl.* 47:10076–80
20. Park HW, Kim ST, Sancar A, Deisenhofer J. 1995. Crystal structure of DNA photolyase from *Escherichia coli*. *Science* 268:1866–72
21. Antony J, Medvedev DM, Stuchebrukhov AA. 2000. Theoretical study of electron transfer between the photolyase catalytic cofactor FADH<sup>-</sup> and DNA thymine dimer. *J. Am. Chem. Soc.* 122:1057–65
22. Sancar A. 1994. Structure and function of DNA photolyase. *Biochemistry* 33:2–9
23. Carell T, Burgdorf LT, Kundu LM, Cichon M. 2001. The mechanism of action of DNA photolyases. *Curr. Opin. Chem. Biol.* 5:491–98
24. Langenbacher T, Zhao XD, Bieser G, Heelis PF, Sancar A, et al. 1997. Substrate and temperature dependence of DNA photolyase repair activity examined with ultrafast spectroscopy. *J. Am. Chem. Soc.* 119:10532–36
25. MacFarlane AW, Stanley RJ. 2003. *Cis-syn* thymidine dimer repair by DNA photolyase in real time. *Biochemistry* 42:8558–68
26. Zhao XD, Liu JQ, Hsu DS, Zhao SY, Taylor JS, et al. 1997. Reaction mechanism of (6-4) photolyase. *J. Biol. Chem.* 272:32580–90
27. Hitomi K, Nakamura H, Kim ST, Mizukoshi T, Ishikawa T, et al. 2001. Role of two histidines in the (6-4) photolyase reaction. *J. Biol. Chem.* 276:10103–9
28. Yamamoto J, Hitomi K, Hayashi R, Getzoff ED, Iwai S. 2009. Role of the carbonyl group of the (6-4) photoproduct in the (6-4) photolyase reaction. *Biochemistry* 48:9306–12
29. Schleicher E, Hitomi K, Kay CWM, Getzoff ED, Todo T, et al. 2007. Electron nuclear double resonance differentiates complementary roles for active site histidines in (6-4) photolyase. *J. Biol. Chem.* 282:4738–47
30. Kao Y-T, Saxena C, Wang L, Sancar A, Zhong D. 2005. Direct observation of thymine dimer repair in DNA by photolyase. *Proc. Natl. Acad. Sci. USA* 102:16128–32
31. Kao Y-T, Saxena C, Wang L, Sancar A, Zhong D. 2007. Femtochemistry in enzyme catalysis: DNA photolyase. *Cell Biochem. Biophys.* 48:32–44
32. Zhong D. 2007. Ultrafast catalytic processes in enzymes. *Curr. Opin. Chem. Biol.* 11:174–81
33. Kao Y-T, Tan C, Song SH, Ozturk N, Li J, et al. 2008. Ultrafast dynamics and anionic active states of the flavin cofactor in cryptochrome and photolyase. *J. Am. Chem. Soc.* 130:7695–701
34. Liu Z, Tan C, Guo X, Kao Y-T, Li J, et al. 2011. Dynamics and mechanism of cyclobutane pyrimidine dimer repair by DNA photolyase. *Proc. Natl. Acad. Sci. USA* 108:14831–36
35. Thiagarajan V, Byrdin M, Eker APM, Muller P, Brettel K. 2011. Kinetics of cyclobutane thymine dimer splitting by DNA photolyase directly monitored in the UV. *Proc. Natl. Acad. Sci. USA* 108:9402–7
36. Liu Z, Guo X, Tan C, Li J, Kao Y-T, et al. 2012. Electron tunneling pathways and role of adenine in repair of cyclobutane pyrimidine dimer by DNA photolyase. *J. Am. Chem. Soc.* 134:8104–14

37. Liu Z, Zhang M, Guo X, Tan C, Li J, et al. 2013. Dynamic determination of the functional state in photolyase and the implication for cryptochrome. *Proc. Natl. Acad. Sci. USA* 110:12972–77
38. Li J, Liu Z, Tan C, Guo X, Wang L, et al. 2010. Dynamics and mechanism of repair of ultraviolet-induced (6-4) photoproduct by photolyase. *Nature* 466:887–90
39. Tan C, Liu Z, Li J, Guo X, Wang L, et al. 2014. Molecular origin of high DNA-repair efficiency by photolyase. Manuscript in review
40. Masson F, Laino T, Rothlisberger U, Hutter J. 2009. A QM/MM investigation of thymine dimer radical anion splitting catalyzed by DNA photolyase. *ChemPhysChem* 10:400–10
41. Borg OA, Eriksson LA, Durbeej B. 2007. Electron-transfer induced repair of 6-4 photoproducts in DNA: a computational study. *J. Phys. Chem. A* 111:2351–61
42. Domratcheva T, Schlichting I. 2009. Electronic structure of (6-4) DNA photoproduct repair involving a non-oxetane pathway. *J. Am. Chem. Soc.* 131:17793–99
43. Sadeghian K, Bocola M, Merz T, Schutz M. 2010. Theoretical study on the repair mechanism of the (6-4) photolesion by the (6-4) photolyase. *J. Am. Chem. Soc.* 132:16285–95
44. Faraji S, Dreuw A. 2012. Proton-transfer-steered mechanism of photolesion repair by (6-4)-photolyases. *J. Phys. Chem. Lett.* 3:227–30
45. Harrison CB, O'Neil LL, Wiest O. 2005. Computational studies of DNA photolyase. *J. Phys. Chem. A* 109:7001–12
46. Faraji S, Dreuw A. 2014. Physicochemical mechanism of light-driven DNA repair by (6-4) photolyases. *Annu. Rev. Phys. Chem.* 65:275–92
47. Ueda T, Kato A, Kuramitsu S, Terasawa H, Shimada I. 2005. Identification and characterization of a second chromophore of DNA photolyase from *Thermus thermophilus* HB27. *J. Biol. Chem.* 280:36237–43
48. Fujihashi M, Numoto N, Kobayashi Y, Mizushima A, Tsujimura M, et al. 2007. Crystal structure of archaeal photolyase from *Sulfolobus tokodaii* with two FAD molecules: implication of a novel light-harvesting cofactor. *J. Mol. Biol.* 365:903–10
49. Kim ST, Heelis PF, Okamura T, Hirata Y, Mataga N, et al. 1991. Determination of rates and yields of interchromophore (folate → flavin) energy transfer and intermolecular (flavin → DNA) electron transfer in *Escherichia coli* photolyase by time-resolved fluorescence and absorption spectroscopy. *Biochemistry* 30:11262–70
50. Jorns MS, Wang BY, Jordan SP, Chanderkar LP. 1990. Chromophore function and interaction in *Escherichia coli* DNA photolyase: reconstitution of the apoenzyme with pterin and/or flavin derivatives. *Biochemistry* 29:552–61
51. Saxena C, Sancar A, Zhong D. 2004. Femtosecond dynamics of DNA photolyase: energy transfer of antenna initiation and electron transfer of cofactor reduction. *J. Phys. Chem. B* 108:18026–33
52. Tan C, Guo L, Ai Y, Li J, Wang L, et al. 2014. Direct determination of resonance energy transfer in photolyase: structural alignment for the functional state. *J. Phys. Chem. A* 118:10522–30
53. Harbach PHP, Schneider M, Faraji S, Dreuw A. 2013. Intermolecular coulombic decay in biology: the initial electron detachment from FADH<sup>-</sup> in DNA photolyases. *J. Phys. Chem. Lett.* 4:943–49
54. Stevens JA, Link JJ, Zang C, Wang L, Zhong D. 2012. Ultrafast dynamics of nonequilibrium resonance energy transfer and probing globular protein flexibility of myoglobin. *J. Phys. Chem. A* 116:2610–19
55. Chang C-W, Guo L, Kao Y-T, Li J, Tan C, et al. 2010. Ultrafast solvation dynamics at binding and active sites of photolyases. *Proc. Natl. Acad. Sci. USA* 107:2914–19
56. Zheng XH, Garcia J, Stuchebrukhov AA. 2008. Theoretical study of excitation energy transfer in DNA photolyase. *J. Phys. Chem. B* 112:8724–29
57. Tamada T, Kitadokoro K, Higuchi Y, Inaka K, Yasui A, et al. 1997. Crystal structure of DNA photolyase from *Anacystis nidulans*. *Nat. Struct. Biol.* 4:887–91
58. Aubert C, Vos MH, Mathis P, Eker APM, Brettel K. 2000. Intraprotein radical transfer during photoactivation of DNA photolyase. *Nature* 405:586–90
59. Byrdin M, Eker APM, Vos MH, Brettel K. 2003. Dissection of the triple tryptophan electron transfer chain in *Escherichia coli* DNA photolyase: Trp382 is the primary donor in photoactivation. *Proc. Natl. Acad. Sci. USA* 100:8676–81

60. Byrdin M, Lukacs A, Thiagarajan V, Eker APM, Brettel K, et al. 2010. Quantum yield measurements of short-lived photoactivation intermediates in DNA photolyase: toward a detailed understanding of the triple tryptophan electron transfer chain. *J. Phys. Chem. A* 114:3207–14
61. Wang H, Saxena C, Quan D, Sancar A, Zhong D. 2005. Femtosecond dynamics of flavin cofactor in DNA photolyase: radical reduction, local solvation, and charge recombination. *J. Phys. Chem. B* 109:1329–33
62. Liu Z, Tan C, Guo X, Li J, Wang L, et al. 2014. Dynamic determination of active-site reactivity in semiquinone photolyase by the cofactor photoreduction. *J. Phys. Chem. Lett.* 5:820–25
63. Liu Z, Tan C, Guo X, Li J, Wang L, et al. 2013. Determining complete electron flow in the cofactor photoreduction of oxidized photolyase. *Proc. Natl. Acad. Sci. USA* 110:12966–71
64. Brazard J, Usman A, Lacombe F, Ley C, Martin MM, et al. 2010. Spectro-temporal characterization of the photoactivation mechanism of two new oxidized cryptochrome/photolyase photoreceptors. *J. Am. Chem. Soc.* 132:4935–45
65. Song SH, Ozturk N, Denaro TR, Arat NO, Kao Y-T, et al. 2007. Formation and function of flavin anion radical in cryptochrome 1 blue-light photoreceptor of monarch butterfly. *J. Biol. Chem.* 282:17608–12
66. Rodgers CT, Hore PJ. 2009. Chemical magnetoreception in birds: the radical pair mechanism. *Proc. Natl. Acad. Sci. USA* 106:353–60
67. Ozturk N, Selby CP, Annayev Y, Zhong D, Sancar A. 2011. Reaction mechanism of *Drosophila* cryptochrome. *Proc. Natl. Acad. Sci. USA* 108:516–21
68. Ozturk N, Song SH, Ozgur S, Selby CP, Morrison L, et al. 2007. Structure and function of animal cryptochromes. *Cold Spring Harb. Symp. Quant. Biol.* 72:119–31
69. Chaves I, Pokorný R, Byrdin M, Hoang N, Ritz T, et al. 2011. The cryptochromes: blue light photoreceptors in plants and animals. *Annu. Rev. Plant Biol.* 62:335–64
70. Li X, Wang Q, Yu X, Liu H, Yang H, et al. 2011. Arabidopsis cryptochrome 2 (CRY2) functions by the photoactivation mechanism distinct from the tryptophan (trp) triad-dependent photoreduction. *Proc. Natl. Acad. Sci. USA* 108:20844–49
71. Liu B, Liu HT, Zhong D, Lin C. 2010. Searching for a photocycle of the cryptochrome photoreceptors. *Curr. Opin. Plant Biol.* 13:578–86
72. Brautigam CA, Smith BS, Ma ZQ, Palnitkar M, Tomchick DR, et al. 2004. Structure of the photolyase-like domain of cryptochrome 1 from *Arabidopsis thaliana*. *Proc. Natl. Acad. Sci. USA* 101:12142–47
73. Levy C, Zoltowski BD, Jones AR, Vaidya AT, Top D, et al. 2013. Updated structure of *Drosophila* cryptochrome. *Nature* 495:E3–4
74. Schmalen I, Reischl S, Wallach T, Klemz R, Grudziecki A, et al. 2014. Interaction of circadian clock proteins CRY1 and PER2 is modulated by zinc binding and disulfide bond formation. *Cell* 157:1203–15
75. Sumi H, Marcus RA. 1986. Dynamic effects in electron transfer reactions. *J. Chem. Phys.* 84:4894–914
76. Wang H, Lin S, Allen JP, Williams JC, Blankert S, et al. 2007. Protein dynamics control the kinetics of initial electron transfer in photosynthesis. *Science* 316:747–50
77. Zhang L, Wang L, Kao Y-T, Qiu W, Yang Y, et al. 2007. Mapping hydration dynamics around a protein surface. *Proc. Natl. Acad. Sci. USA* 104:18461–66
78. Zhang L, Yang Y, Kao Y-T, Wang L, Zhong D. 2009. Protein hydration dynamics and molecular mechanism of coupled water-protein fluctuations. *J. Am. Chem. Soc.* 131:10677–91
79. Zhong D. 2009. Hydration dynamics and coupled water-protein fluctuations probed by intrinsic tryptophan. *Adv. Chem. Phys.* 143:83–149
80. Zhong D, Pal SK, Zewail AH. 2011. Biological water: a critique. *Chem. Phys. Lett.* 503:1–11
81. Qin Y, Yang Y, Zhang L, Fowler JD, Qiu W, et al. 2013. Direct probing of solvent accessibility and mobility at the binding interface of polymerase (Dpo4)-DNA complex. *J. Phys. Chem. A* 117:13926–34
82. Chang C-W, He T-F, Guo L, Stevens JA, Li T, et al. 2010. Mapping solvation dynamics at the functional site of flavodoxin in three redox states. *J. Am. Chem. Soc.* 132:12741–47
83. Barbara PF, Meyer TJ, Ratner MA. 1996. Contemporary issues in electron transfer research. *J. Phys. Chem.* 100:13148–68

84. Nagasawa Y, Yartsev AP, Tominaga K, Bisht PB, Johnson AE, Yoshihara K. 1995. Dynamical aspects of ultrafast intermolecular electron transfer faster than solvation process: substituent effects and energy gap dependence. *J. Phys. Chem.* 99:653–62
85. LeBard DN, Kapko V, Matyushov DV. 2008. Energetics and kinetics of primary charge separation in bacterial photosynthesis. *J. Phys. Chem. B* 112:10322–42
86. He T-F, Guo L, Guo X, Chang C-W, Wang L, et al. 2013. Femtosecond dynamics of short-range protein electron transfer in flavodoxin. *Biochemistry* 52:9120–28
87. Jorns MS, Sancar GB, Sancar A. 1985. Identification of oligothymidylates as new simple substrates for *Escherichia coli* DNA photolyase and their use in a rapid spectrophotometric enzyme assay. *Biochemistry* 24:1856–61
88. Hassanali AA, Zhong D, Singer SJ. 2011. An AIMD study of the CPD repair mechanism in water: reaction free energy surface and mechanistic implications. *J. Phys. Chem. B* 115:3848–59
89. Hassanali AA, Zhong D, Singer SJ. 2011. An AIMD study of CPD repair mechanism in water: role of solvent in ring splitting. *J. Phys. Chem. B* 115:3860–71
90. Shih C, Museth AK, Abrahamsson M, Blanco-Rodriguez AM, Di Bilio AJ, et al. 2008. Tryptophan-accelerated electron flow through proteins. *Science* 320:1760–62
91. Stubbe J, Nocera DG, Yee CS, Chang MCY. 2003. Radical initiation in the class I ribonucleotide reductase: long-range proton-coupled electron transfer? *Chem. Rev.* 103:2167–201
92. Prytkova TR, Kurnikov IV, Beratan DN. 2007. Coupling coherence distinguishes structure sensitivity in protein electron transfer. *Science* 315:622–25
93. Medvedev D, Stuchebrukhov AA. 2001. DNA repair mechanism by photolyase: electron transfer path from the photolyase catalytic cofactor FADH<sup>-</sup> to DNA thymine dimer. *J. Theor. Biol.* 210:237–48
94. Prytkova TR, Beratan DN, Skourtis SS. 2007. Photoselected electron transfer pathways in DNA photolyase. *Proc. Natl. Acad. Sci. USA* 104:802–7
95. Acocella A, Jones GA, Zerbetto F. 2010. What is adenine doing in photolyase? *J. Phys. Chem. B* 114:4101–6
96. Wang H, Chen X, Fang W. 2014. Excited-state proton coupled electron transfer between photolyase and the damaged DNA through water wire: a photo-repair mechanism. *Phys. Chem. Chem. Phys.* 16:25432–41
97. Zhong D, Sancar A, Stuchebrukhov A. 2012. Reply to Brettel and Byrdin: on the efficiency of DNA repair by photolyase. *Proc. Natl. Acad. Sci. USA* 109:E1463
98. Kao Y-T, Saxena C, He T-F, Guo L, Wang L, et al. 2008. Ultrafast dynamics of flavins in five redox states. *J. Am. Chem. Soc.* 130:13132–39
99. Moonen CTW, Vervoort J, Muller F. 1984. Reinvestigation of the structure of oxidized and reduced flavin: carbon-13 and nitrogen-15 nuclear magnetic resonance study. *Biochemistry* 23:4859–67
100. Zheng Y-J, Ornstein RL. 1996. A theoretical study of the structures of flavin in different oxidation and protonation states. *J. Am. Chem. Soc.* 118:9402–8
101. Huels MA, Boudaiffa B, Cloutier P, Hunting D, Sanche L. 2003. Single, double, and multiple double strand breaks induced in DNA by 3–100 eV electrons. *J. Am. Chem. Soc.* 125:4467–77
102. Kim ST, Hartman RF, Rose SD. 1990. Solvent dependence of pyrimidine dimer splitting in a covalently linked dimer-indole system. *Photochem. Photobiol.* 52:789–94
103. Tang WJ, Guo QX, Song Q-H. 2009. Origin of solvent dependence of photosensitized splitting of a cyclobutane pyrimidine dimer by a covalently linked chromophore. *J. Phys. Chem. B* 113:7205–10
104. Kao Y-T, Song Q-H, Saxena C, Wang L, Zhong D. 2012. Dynamics and mechanism of DNA repair in a biomimetic system: flavin-thymine dimer adduct. *J. Am. Chem. Soc.* 134:1501–3
105. Kim ST, Li YF, Sancar A. 1992. The third chromophore of DNA photolyase: Trp-277 of *Escherichia coli* DNA photolyase repairs thymine dimers by direct electron transfer. *Proc. Natl. Acad. Sci. USA* 89:900–4
106. Vivic DA, Odom DT, Núñez ME, Gianolio DA, McLaughlin LW, et al. 2000. Oxidative repair of a thymine dimer in DNA from a distance by a covalently linked organic intercalator. *J. Am. Chem. Soc.* 122:8603–11
107. Yamamoto J, Martin R, Iwai S, Plaza P, Brettel K. 2013. Repair of the (6-4) photoproduct by DNA photolyase requires two photons. *Angew. Chem. Int. Ed. Engl.* 52:7432–36
108. Yamamoto J, Tanaka Y, Iwai S. 2009. Spectroscopic analysis of the pyrimidine(6-4)pyrimidone photoproduct: insights into the (6-4) photolyase reaction. *Org. Biomol. Chem.* 7:161–66

109. Glas AF, Schneider S, Maul MJ, Hennecke U, Carell T. 2009. Crystal structure of the T(6-4)C lesion in complex with a (6-4) DNA photolyase and repair of UV-induced (6-4) and Dewar photolesions. *Chem. Eur. J.* 15:10387–96
110. Guo X, Liu Z, Song Q, Wang L, Zhong D. 2015. Dynamics and mechanism of UV-damaged DNA repair in indole-thymine dimer adduct: molecular origin of low repair quantum efficiency. *J. Phys. Chem. B* 119:3446–55